Study of Inclusive Strange-Baryon Production and Search for Pentaquarks in Two-Photon Collisions at LEP

The L3 Collaboration

Abstract

Measurements of inclusive production of the Λ, Ξ^- and $\Xi^*(1530)$ baryons in two-photon collisions with the L3 detector at LEP are presented. The inclusive differential cross sections for Λ and Ξ^- are measured as a function of the baryon transverse momentum, p_t, and pseudo-rapidity, η. The mean number of Λ, Ξ^- and $\Xi^*(1530)$ baryons per hadronic two-photon event is determined in the kinematic range 0.4 GeV $< p_t <$ 2.5 GeV, $|\eta| < 1.2$. Overall agreement with the theoretical models and Monte Carlo predictions is observed. A search for inclusive production of the pentaquark $\theta^+(1540)$ in two-photon collisions through the decay $\theta^+ \to pK_S^0$ is also presented. No evidence for production of this state is found.

1 Introduction

Two-photon collisions are the main source of hadron production in high-energy e^+e^- interactions at LEP, via the process $e^+e^- \rightarrow e^+e^-\gamma^*\gamma^* \rightarrow e^+e^-hadrons$, for which the cross section is many orders of magnitude larger than the e^+e^- annihilation cross section. The outgoing electron and positron carry almost the full beam energy and their transverse momenta are usually so small that they escape undetected along the beam pipe. At the LEP energies considered here, the negative four-momentum squared of the photons, Q^2, has an average value of $\langle Q^2 \rangle \simeq 0.2$ GeV^2. Therefore, the photons may be considered as "quasi-real". In the Vector Dominance Model (VDM), each virtual photon can fluctuate into a vector meson, thus initiating a strong interaction process with characteristics similar to hadron-hadron interactions. This process dominates in the "soft" interaction region, where hadrons are produced with a low transverse momentum, p_t. Hadrons with high p_t are instead mainly produced by the QED process $\gamma\gamma \rightarrow q\bar{q}$ (direct process) or by QCD processes originating from the partonic content of the photon (resolved processes).

Fragmentation mechanisms can be investigated in two-photon reactions. These processes are described phenomenologically. In the Lund string model [1], hadron production proceeds through the creation of quark-antiquark and diquark-antidiquark pairs during string fragmentation. Mesons and baryons are formed by colorless quark-antiquark and quark-diquark combinations, respectively. An extension of this model, the "simple popcorn mechanism" [2], includes the possibility of producing an additional meson between baryon-antibaryon pairs. The relative rate of occurrence of the baryon-meson-antibaryon configuration is governed by the so called "popcorn parameter." Many other parameters must be tuned to reproduce the measured hadron production rate, such as the strange-quark suppression factor, the diquark-to-quark production ratio or the spin-1 diquark suppression factor.

In a statistical model approach [3], hadronisation is described with a reduced number of free parameters. Particles are produced in a purely statistical way from a massive colourless gas which, for hadron production in two-photon collisions, is completely specified by two parameters: the energy density (or temperature) and a strange-quark suppression factor. In this model, the yield of different particles depends only on their masses, spins and quantum numbers.

The L3 Collaboration has previously measured inclusive π^0, K_S^0 and Λ production in quasi-real two-photon collisions for a centre-of-mass energy of the two interacting photons, $W_{\gamma\gamma}$, greater than 5 GeV [4, 5]. In this Article this study is extended to the Ξ^-, $\Xi^*(1530)$ and Ω^- baryons[1]. The data sample consists of a total integrated luminosity of 610 pb^{-1}, collected with the L3 detector [6] at e^+e^- centre-of-mass energies $\sqrt{s} = 189 - 209$ GeV, with a luminosity weighted average value $\langle\sqrt{s}\rangle = 198$ GeV. Inclusive strange-baryon production has been extensively studied in e^+e^- annihilation processes [7], whereas in two-photon collisions only inclusive Λ production has been previously measured at lower $\sqrt{s}$ by the TOPAZ Collaboration [8].

Heavy-baryon detection techniques are also applied to search for pentaquark production in two-photon interactions, using the decay channel $\theta^+ \rightarrow pK_S^0$. Since the first observation of a narrow resonance near 1540 MeV in the K^+n mass spectrum [9], interpreted as the pentaquark θ^+, experimental evidence for and against this new state has been accumulated [10]. Second-generation experiments have so far not confirmed the existence of this state [11]. No search in two-photon reactions has been performed yet.

---

[1] If not stated otherwise, the symbols Λ, Ξ^- and Ω^- refer to both the Λ, Ξ^- and Ω^- as well as $\overline{\Lambda}$, $\overline{\Xi}^+$ and $\overline{\Omega}^+$ baryons. All charge-conjugate final-states are analysed.

2 Monte Carlo simulation

The process $e^+e^- \to e^+e^- hadrons$ is modelled with the PYTHIA [12] and PHOJET [13] event generators with twice the statistics of the data. In PYTHIA, each photon is classified as direct, VDM or resolved, leading to six classes of two-photon events. A smooth transition between these classes is obtained by introducing a p_t parameter to specify the boundaries. The SaS-1D parametrization is used for the photon parton density function [14]. Since both incoming photons are assumed to be real in the original program, PYTHIA is modified to generate a photon flux according to the equivalent photon approximation [15] with an upper Q^2 cut at the mass squared of the rho meson.

PHOJET is a general purpose Monte Carlo which describes hadron-hadron, photon-hadron and photon-photon collisions. It relies on the dual parton model combined with the QCD-improved parton model [16]. The p_t distribution of the soft partons is matched to the one predicted by QCD to ensure a continuous transition between hard and soft processes. The two-photon luminosity function is calculated in the formalism of Reference 15. The leading-order GRV parametrisation is used for the photon parton density function [17].

In both programs, matrix elements and hard scattering processes are calculated at the leading order and higher-order terms are approximated by a parton shower in the leading-log approximation. The fragmentation is performed within the Lund string fragmentation scheme as implemented in JETSET [12], which is also used to simulate the hadronisation process. JETSET parameters are tuned by using hadronic Z decays [18]. In particular, the strangeness-suppression factor is set to 0.3, whereas the parameter governing the extra suppression of strange quarks in diquarks is fixed to 0.4 and the diquark-to-quark production ratio to 0.10. The popcorn parameter is set to 0.5 and a value $\alpha_S(m_Z) = 0.12$ is used for the strong coupling-constant.

The following Monte Carlo generators are used to simulate the background processes: KK2f [19] for the annihilation process $e^+e^- \to q\overline{q}(\gamma)$; KORALZ [20] for $e^+e^- \to \tau^+\tau^-(\gamma)$; KORALW [21] for $e^+e^- \to W^+W^-$ and DIAG36 [22] for $e^+e^- \to e^+e^-\tau^+\tau^-$. The response of the L3 detector is simulated using the GEANT [23] and GHEISHA [24] programs. Time-dependent detector inefficiencies, as monitored during each data-taking period, are included in the simulations. All simulated events are passed through the same reconstruction program as the data.

3 Two-photon event selection

Two-photon interaction events are mainly collected by track triggers [25], with a track p_t threshold of about 150 MeV, and the calorimetric energy trigger [26]. The selection of $e^+e^- \to e^+e^- hadrons$ events [27] is based on information from the central tracking detectors and the electromagnetic and hadronic calorimeters. It consists of:

- A multiplicity cut. To select hadronic final states, at least six objects must be detected, where an object can be a track satisfying minimal quality requirements or an isolated cluster in the BGO electromagnetic calorimeter of energy greater than 100 MeV.

- Energy cuts. The total energy deposited in the calorimeters must be less than 40% of $\sqrt{s}$ to suppress events from the $e^+e^- \to q\overline{q}(\gamma)$ and $e^+e^- \to \tau^+\tau^-(\gamma)$ processes. In addition, the total energy in the electromagnetic calorimeter is required to be greater than 500 MeV

to suppress beam-gas and beam-wall interactions and less than 50 GeV to remove events from the annihilation process $e^+e^- \to q\bar{q}(\gamma)$.

- An anti-tag condition. Events containing a cluster in the luminosity monitor with an electromagnetic shower shape, and energy greater than 30 GeV, are excluded from the analysis. The luminosity monitor covers the polar angular region 31 mrad $< \theta <$ 62 mrad on both sides of the detector. In addition, events with an electron or positron scattered above 62 mrad are rejected by the cut on calorimetric energy.

- A mass cut. The mass of all visible particles, W_{vis}, must be greater than 5 GeV to exclude the resonance region. In this calculation, the pion mass is attributed to tracks while isolated electromagnetic clusters are treated as massless.

About 3 million hadronic events are selected by these criteria with an overall efficiency of 45% for a two-photon centre-of-mass energy, $W_{\gamma\gamma}$, greater than 5 GeV. The background level of this sample is less than 1% and is mainly due to the $e^+e^- \to q\bar{q}(\gamma)$ and $e^+e^- \to e^+e^-\tau^+\tau^-$ processes. The backgrounds from beam-gas and beam-wall interactions are negligible.

4 Strange baryon selection

The Λ, Ξ^- and Ω^- baryons are identified through the decays $\Lambda \to p\pi^-$, $\Xi^- \to \Lambda\pi^-$ and $\Omega^- \to \Lambda K^-$. Due to their long lifetimes, the combinatorial background can be strongly suppressed by selecting secondary vertices which are clearly displaced from the interaction point. The $\Xi^*(1530)$ decays strongly into $\Xi^-\pi^+$ and no corresponding displaced vertex can be observed.

The Ξ^-, Ω^- and $\Xi^*(1530)$ final states are reconstructed by combining Λ candidates with pion or kaon candidates. The latter are defined as tracks formed by at least 30 hits in the central tracker out of a maximum of 62 and a $p_t > 100$ MeV. The probability of the pion or kaon hypothesis, based on the dE/dx measurement in the tracking chamber, is required to be greater than 0.01.

4.1 Λ selection

The selection procedure is unchanged from our previous publication [5]. The Λ identification is optimized to achieve a high efficiency and a good background suppression by selecting secondary decay vertices satisfying the following conditions:

- The distance d_Λ in the transverse plane[2)] between the secondary vertex and the e^+e^- interaction point must be greater than 3 mm.

- The angle α_Λ between the sum p_t vector of the two tracks and the direction in the transverse plane between the e^+e^- interaction point and the secondary vertex must be less than 100 mrad.

The distributions of these variables are presented in Figure 1. Good agreement between data and Monte Carlo is observed. The proton is identified as the track with the largest momentum, an assignment shown by Monte Carlo to be correct more than 99% of the time. The dE/dx

---

[2)]The transverse plane is defined as the plane transverse to the beam direction.

4

measurements in the central tracking chamber must be consistent with this assignment, a probability greater than 0.01 for both the proton and the pion candidates being required.

The distribution of the corresponding invariant mass of the pπ system, $m(\mathrm{p}\pi)$, is shown in Figure 2a. A clear Λ peak over a smooth background is visible, compatible with the Λ baryon mass, $m_\Lambda = 1115.68 \pm 0.01$ MeV [7]. The resolution of the signal, about 3 MeV, is well reproduced by Monte Carlo simulation. The $m(\mathrm{p}\pi)$ mass spectrum for the pπ^- and $\overline{\mathrm{p}}\pi^+$ combinations are shown in Figure 2b and 2c, respectively. The numbers of Λ baryons for different p_t and $|\eta|$ bins are given in Tables 1 and 2. They are determined by a fit in which the signal is modelled by a Gaussian and the background by a fourth-order Chebyshev polynomial. Consistent values of the fitted mass and width are found for the different p_t and $|\eta|$ bins.

4.2 Ξ^- selection

The Ξ^- baryons are reconstructed by combining Λ candidates with pion candidates. For the identification of Ξ^- and Ω^- baryons, different criteria are used to select secondary vertices produced by Λ decays. The distance d_Λ is required to be greater than 5 mm and the angle α_Λ less than 200 mrad, as shown in Figure 3a and 3b. The other cuts are left unchanged. The distribution of the resulting invariant mass $m(\mathrm{p}\pi)$ is displayed in Figure 3c and shows a clear Λ peak. The 76000 pπ combinations that lie in the mass interval 1.105 GeV $< m(\mathrm{p}\pi) <$ 1.125 GeV are retained. To reduce the combinatorial background, the following criteria are applied:

- the distance of closest approach (DCA) in the transverse plane of the Ξ^- decay pion to the e$^+$e$^-$ interaction point, d_π, must be greater than 1 mm.

- the distance in the transverse plane between the $\Lambda\pi$ vertex and the e$^+$e$^-$ interaction point, d_Ξ, is required to be greater than d_Λ.

- the angle α_Ξ between the p_t vector of the $\Lambda\pi$ combination and the direction in the transverse plane between the e$^+$e$^-$ interaction point and the $\Lambda\pi$ vertex has to be less than 100 mrad.

Distributions of the difference $d_\Lambda - d_\Xi$ and of the angle α_Ξ are displayed in Figure 4 and exhibit a good agreement with the Monte Carlo predictions.

The distribution of the mass of the $\Lambda\pi$ system, $m(\Lambda\pi)$, is displayed in Figure 5 for the $\Lambda\pi^-$ and $\overline{\Lambda}\pi^+$ combinations, respectively. Figure 6 shows the $m(\Lambda\pi)$ spectrum for the different p_t bins listed in Table 1. A clear Ξ^- peak is visible over a smooth background, compatible with the measured Ξ^- mass, $m_{\Xi^-} = 1321.31 \pm 0.13$ MeV [7]. The resolution of $m(\Lambda\pi)$, about 7 MeV, is well reproduced by Monte Carlo simulation. The number of Ξ^- baryons in each p_t and $|\eta|$ bin is evaluated by means of a fit to the $m(\Lambda\pi)$ spectrum in the interval 1.26 GeV $< m(\mathrm{p}\pi) <$ 1.4 GeV. The signal is modelled with a Gaussian and the background by a fourth-order Chebyshev polynomial. The results are listed in Tables 1 and 2.

4.3 $\Xi^*(1530)$ selection

The $\Xi^*(1530)$ baryons are identified by reconstructing the decays $\Xi^*(1530) \to \Xi^-\pi^+$ and $\Xi^*(1530) \to \overline{\Xi}^+\pi^-$. The Ξ^- candidates with a mass of ± 15 MeV around the nominal Ξ^- mass are combined with pion candidates. As the latter are produced at the e$^+$e$^-$ interaction point, their DCA must be less than 5 mm. To compare the $\Xi^*(1530)$ production to other strange

baryons, the measurement is restricted to the kinematical region: 0.4 GeV $< p_t < 2.5$ GeV, $|\eta| < 1.2$. The distribution of the invariant mass of the $\Xi\pi$ system, $m(\Xi\pi)$, is shown in Figure 7a for opposite-charge ($\Xi^-\pi^+$ and $\overline{\Xi}^+\pi^-$) and same-charge ($\Xi^-\pi^-$ and $\overline{\Xi}^+\pi^+$) combinations. The number of same-charge combinations is normalized to that of opposite-charge combinations in the region $m(\Xi\pi) > 1.7$ GeV. An excess corresponding to the $\Xi^*(1530)$ is observed in the opposite-charge spectrum close to the nominal mass $m_{\Xi^*(1530)} = 1531.80 \pm 0.32$ MeV [7]. The number of $\Xi^*(1530)$ baryons is determined by means of a fit to the mass spectrum in the region 1.47 GeV $< m(\Xi\pi) < 1.90$ GeV, as shown in Figure 7b. The signal is modelled with a Gaussian and the background is parametrized by a threshold function of the form:

$$a(m_{(\Xi\pi)} - m_0)^b \, \exp\left[c(m_{(\Xi\pi)} - m_0) + d(m_{(\Xi\pi)} - m_0)^2\right]$$

where a, b, c, d and m_0 are free parameters. The results are given in Table 1.

4.4 Search for Ω^-

Since the topology of the $\Omega^- \to \Lambda K^-$ decay is similar to that of $\Xi^- \to \Lambda\pi^-$, the selection criteria are identical except that kaon candidates are combined with Λ candidates instead of pion candidates. The corresponding $m(\Lambda K)$ spectrum is displayed in Figure 8. No signal is observed around the nominal mass of the Ω^- baryon, $m_{\Omega^-} = 1672.45 \pm 0.29$ MeV [7]. The expected signal, as predicted by PHOJET, is found to be almost negligible.

5 Results and systematic uncertainties

The cross sections for Λ, Ξ^- and $\Xi^*(1530)$ production are measured for $W_{\gamma\gamma} > 5$ GeV, with a mean value $\langle W_{\gamma\gamma}\rangle = 30$ GeV, and a photon virtuality $Q^2 < 8$ GeV^2 with $\langle Q^2\rangle \simeq 0.2$ GeV^2. This kinematical region is defined by cuts at Monte Carlo generator level.

The overall efficiencies for detecting Λ, Ξ^- and $\Xi^*(1530)$ baryons as a function of p_t and $|\eta|$ are listed in Tables 1 and 2. They include reconstruction and trigger efficiencies as well as branching fractions for the decays $\Xi^*(1530) \to \Xi^-\pi^+$, $\Xi^- \to \Lambda\pi^-$ and $\Lambda \to p\pi^-$: 67%, 100% and 64%, respectively [7]. The reconstruction efficiencies, which include effects of the acceptance and the selection cuts, are calculated with the PHOJET and PYTHIA Monte Carlo generators. As both generators reproduce well the shapes of the experimental distributions of hadronic two-photon production [27], the average selection efficiency is used. The track-trigger efficiency is calculated for each data-taking period by comparing the number of events accepted by the track triggers and the independant calorimetric-energy triggers. The efficiency of the higher level triggers is measured using prescaled events. The total trigger efficiency varies from 82% for $p_t < 0.4$ GeV to 85% in the high p_t region.

The differential cross sections $d\sigma/dp_t$, $d\sigma/dp_t^2$ and $d\sigma/d|\eta|$ for the reactions $e^+e^- \to e^+e^-\Lambda X$ and $e^+e^- \to e^+e^-\Xi^- X$ are given in Table 1 and Table 2, respectively. The mean number of Λ, Ξ^- and $\Xi^*(1530)$ baryons per hadronic two-photon event is measured in the region 0.4 GeV $< p_t < 2.5$ GeV, $|\eta| < 1.2$ and $W_{\gamma\gamma} > 5$ GeV, as summarized in Table 3. Finally, the ratio of Λ to $\overline{\Lambda}$ and Ξ^- to $\overline{\Xi}^+$ baryons are determined from the respective mass spectra. They are found to be $N(\overline{\Lambda})/N(\Lambda) = 0.99 \pm 0.04$ and $N(\overline{\Xi}^+)/N(\Xi^-) = 0.96 \pm 0.14$, where the uncertainties are statistical. These results are in agreement with the value of 1.0 expected for baryon pair production in two-photon reactions.

The following sources of systematic uncertainties are considered: selection procedure, background subtraction, limited Monte Carlo statistics, Monte Carlo modelling and the accuracy

of the trigger efficiency measurement. Their contributions to the cross section measurements are detailed in Table 4.

The uncertainties associated to the selection criteria are evaluated by changing the corresponding cuts and repeating the fitting procedure. The Λ selection uncertainty is dominated by the secondary vertex identification while the largest uncertainty for the Ξ^- channel, about 9%, arises from the $\Lambda\pi$ vertex reconstruction. The uncertainty due to the $e^+e^- \to e^+e^-$ *hadrons* event selection is less than 1%.

The uncertainty due to background subtraction is assessed by using different background parameterizations and fit intervals in the fitting procedure. The Monte Carlo modelling uncertainty, taken as half the relative difference difference between PHOJET and PYTHIA, varies between 1% and 14% whereas the uncertainty associated to the limited Monte Carlo statistics varies from 1% for Λ to 18% for $\Xi^*(1530)$. A systematic uncertainty of 2% is assigned to the determination of the trigger efficiency, which takes into account the determination procedure and time stability.

6   Comparison with Monte Carlo and theoretical models

The differential cross sections $d\sigma/dp_t^2(e^+e^- \to e^+e^-\Lambda X)$ and $d\sigma/dp_t^2(e^+e^- \to e^+e^-\Xi^-X)$ for $|\eta| < 1.2$ are presented in Figure 9a. The behaviour of the cross sections is well described by an exponential of the form $A\exp(-ap_t^2)$ in the region $0.16\text{ GeV}^2 < p_t^2 < 1.69\text{ GeV}^2$ with $a = 1.78 \pm 0.16\text{ GeV}^{-2}$ and $a = 1.68 \pm 0.35\text{ GeV}^{-2}$ for Λ and Ξ^- production, respectively. These two values are compatible with each other, as expected from the Lund string model. The region $1.69\text{ GeV}^2 < p_t^2 < 6.25\text{ GeV}^2$ is better reproduced by a power law of the form Ap_t^{-b} with $b = 5.2 \pm 0.2$ and $b = 4.2 \pm 0.9$ for Λ and Ξ^- baryons, respectively.

The differential cross sections $d\sigma/dp_t(e^+e^- \to e^+e^-\Lambda X)$ and $d\sigma/dp_t(e^+e^- \to e^+e^-\Xi^-X)$ for $|\eta| < 1.2$ are displayed in Figure 9b. Phase-space suppression explains the lower values obtained in the first bins. The behaviour of the cross sections is well described by an exponential of the form $A\exp(-p_t/\langle p_t\rangle)$ in the region $0.75\text{ GeV} < p_t < 2.5\text{ GeV}$ with a mean value $\langle p_t\rangle = 368 \pm 17\text{ MeV}$ for Λ production and in the range $0.7\text{ GeV} < p_t < 2.5\text{ GeV}$ with $\langle p_t\rangle = 472\pm98\text{ MeV}$ for Ξ^- formation. These values are larger than those obtained for inclusive π^0 and K_S^0 production: $\langle p_t\rangle \simeq 230\text{ MeV}$ and $\langle p_t\rangle \simeq 290\text{ MeV}$, respectively [4].

The data are compared to the PHOJET and PYTHIA Monte Carlo predictions in Figure 10a. Both Monte Carlo programs fail to reproduce the shape and the normalization of the Λ cross section. A better agreement can be achieved by adjusting the width σ_q in the Gaussian p_t distribution for primary hadrons produced during the fragmentation. As shown in Figure 10b, the predictions obtained with PYTHIA for Λ production using a value $\sigma_q = 0.546\text{ GeV}$ reproduce much better the data than those with the default value $\sigma_q = 0.411\text{ GeV}$. On the other hand, an increase of the width of the p_t distribution of quarks inside initial photons does not improve the description of the measured spectra. Similar trends are observed with PHOJET.

The differential cross sections as a function of $|\eta|$ are displayed in Figure 11a and 11b. Both Monte Carlo programs describe well the almost-uniform $|\eta|$ shape, while the size of the discrepancy on the absolute normalization depends on the p_t range.

The mean numbers of Λ, Ξ^- and $\Xi^*(1530)$ baryons per hadronic two-photon event are extrapolated from the measured phase-space to the full p_t and $|\eta|$ range using the PYTHIA Monte Carlo with the adjusted value $\sigma_q = 0.546\text{ GeV}$. The uncertainty on the extrapolation factors propagates to the results as an additional systematic uncertainty. It arises mainly from

the modelling of the two-photon reaction and fragmentation processes. The contribution due to fragmentation, about 7%, is estimated using an independent fragmentation model [28] instead of the Lund string scheme to simulate baryon production as well as varying the parameters of these models. The two-photon modelling uncertainty, taken as the difference between the extrapolation factors estimated by PYTHIA and PHOJET, is found to be 3%. The results are summarized in Table 3 together with the predictions of PYTHIA and PHOJET. Both Monte Carlos overestimate the Λ and Ξ^- mean numbers, the discrepancy being less pronounced in PYTHIA than in PHOJET. A better agreement is obtained by decreasing the strange-quark suppression factor by a few percent. These extrapolated mean numbers can be converted to inclusive cross sections by multiplying them for the total two-photon hadronic cross section measured with the same detector as discussed in Reference [27].

The predictions of the thermodynamical model of Reference 3 are displayed in Figure 12 as a function of the strangeness suppression factor γ_s, using as energy density the value $\rho = 0.4$ [3]. Overall agreement is observed for a γ_s in the vicinity of $\gamma_s = 0.7$, which is similar to the value extracted from e^+e^- annihilation events [29].

As suggested in Reference 30, the mean numbers $\langle n \rangle$ of octet and decuplet baryons can also be parametrized by a function of the form:

$$\langle n \rangle = a\Big[(2J+1)/(2I+1)\Big]\exp(-bm^2)$$

where I, J, m are respectively the isospin, total angular momentum and mass of the baryons and a, b are free parameters. The ratios $\Big[(2J+1)/(2I+1)\Big]\langle n \rangle$ are displayed in Figure 13 together with the data measured in e^+e^- collisions at $\sqrt{s} = 10$ GeV and $\sqrt{s} = 91$ GeV [7]. A fit to our data gives $b = 4.5 \pm 0.9$, a value compatible with the exponents $b = 4.3 \pm 0.6$ and $b = 4.0 \pm 0.1$ obtained for e^+e^- reactions at $\sqrt{s} = 10$ GeV and $\sqrt{s} = 91$ GeV, respectively. This provides evidence for the universality of fragmentation processes in two-photon and e^+e^- reactions.

7 Search for the θ^+ pentaquark

A $\theta^{+3)}$ Monte Carlo consisting of pentaquarks mixed with large samples of hadronic two-photon events is used to study the kinematics of the θ^+ decay products and estimate the signal efficiency. In this Monte Carlo the pentaquarks are generated with a mass of 1.54 GeV and a width of 1 MeV. The transverse momentum and pseudo-rapidity distributions predicted by the PYTHIA event generator for inclusive $\Xi^*(1530)$ production are taken to model the unknown distributions of the pentaquarks. As these distributions are very similar for different low mass baryons, the simulated acceptance is expected to be quite insensitive to the choice of a particular baryon. The $\theta^+ \to pK_S^0$ decay is assumed to be isotropic. The $K_S^0 p$ and $K_S^0 \overline{p}$ mass distributions, calculated at the generator level, show no evidence of a narrow peak close to 1540 MeV. This indicates that no reflections from known decay modes could generate a fake θ^+ signal.

7.1 Event selection

The θ^+ candidates are reconstructed using the decay $\theta^+ \to pK_S^0$. Events are selected if they contain at least one track coming from the e^+e^- interaction point and a K_S^0 decaying into $\pi^+\pi^-$ at a secondary vertex. The K_S^0 selection proceeds as follows:

---

3) If not stated otherwise, the symbols θ^+ refers to θ^+ and $\overline{\theta}^-$ as both charge-conjugate final-states are analysed.

- Each track is required to have more than 12 hits out a maximum of 62 and $p_t > 100$ MeV.

- The dE/dx measurement of both pion candidates must be consistent with this hypothesis with a probability greater than 0.01.

- The distance in the transverse plane between the secondary vertex and the e^+e^- interaction point must be greater than 5 mm.

- The angle between the sum p_t vector of the two tracks and the direction in the transverse plane between the primary interaction point and the secondary vertex must be less than 75 mrad.

The distribution of the effective mass of the $\pi\pi$ system, $m(\pi\pi)$, is shown in Figure 14. A clear K_S^0 peak is present over a smooth background. The spectrum is fitted with two Gaussian functions and a second order polynomial for the background. A central value of 497.6 ± 0.1 MeV is obtained for the peak, which agrees with the expected value of 497.7 MeV [7]. To search for θ^+, the K_S^0 candidates are selected within an interval of ±20 MeV around the central value of the peak, corresponding to 140000 K_S^0 candidates with a purity of 69%.

The proton and antiproton candidates are tracks with at least 30 hits out of a maximum of 62 and a DCA less than 5 mm. In addition, the dE/dx measurement in the central tracker must be consistent with the proton hypothesis with a probability greater than 0.05. To reject kaons and pions, the probability of each of these hypothesis must be less than 0.01. A total of 7131 selected protons and 5340 antiprotons are selected. Their dE/dx measurement is shown in Figure 15 together with theoretical the expectations based on the Bethe-Bloch formula. The purity of the selected sample is greater than 96%. The excess of protons, due to secondary interactions between particles and the detector, is well reproduced by the Monte Carlo.

The resulting pK_S^0 and $\overline{p}K_S^0$ mass spectra, $m(pK_S^0)$, are shown in Figure 16a and 16b respectively. Since no distinct structure due to the excess of protons is observed, the two spectra are combined in the following.

7.2   Results

An upper limit for the number of $e^+e^- \rightarrow e^+e^-\theta^+X$ events at 95% confidence level is derived with a fit to the $m(pK_S^0)$ mass spectrum. To minimize the effect of the binning and the choice of the fitting interval, an unbinned maximum likelihood fit is performed in the range 1.45 GeV $< W_{\gamma\gamma} < 1.8$ GeV. The likelihood function is written as:

$$\mathcal{L} = p \cdot g(m_{(pK_S^0)}) + (1-p) \cdot b(m_{(pK_S^0)})$$

where p denotes the fraction of signal events inside the fitted region. The background, $b(m_{(pK_S^0)})$, is parametrized by a fourth-order polynomial and the signal by a Gaussian distribution, $g(m_{(pK_S^0)})$. The resolution of the expected signal is determined from Monte Carlo to be 14.0 ± 0.6 MeV. The resulting fit is displayed in Figure 17 and yields a fraction of signal events compatible with zero: $p = -0.006 \pm 0.007$. Restricting the measurement to the physical region $p \geq 0$, an upper limit of 59.3 events at 95% confidence level is derived.

The θ^+ selection efficiency is estimated to be 1.0%, including a branching fraction $K_S^0 \rightarrow \pi^+\pi^-$ of 69% [7]. The branching ratio $\theta^+ \rightarrow pK_S^0$ is set to 1/4, accounting for competition with both the K^+n and K_L^0p channels. The overall trigger efficiency is measured to be 83%.

The mean number of θ^+ pentaquark per hadronic two-photon event extrapolated to the full phase-space for $W_{\gamma\gamma} > 5$ GeV is found to be less than 4.0×10^{-3} at 95% confidence level. The systematic uncertainty arising from the selection procedure is evaluated by varying the cuts and repeating the fitting procedure. The contribution of the K_S^0 reconstruction is estimated to be 9% whereas an uncertainty of 4% is associated with proton identification. The uncertainty due to θ^+ modelling, determined by using the p_t and pseudo-rapidity distributions of different baryons in the θ^+ generation, is found to be 9%. The effect of a non-isotropic $\theta^+ \to pK_S^0$ decay on the efficiency is estimated using an angular distribution of the form $1 - \cos^2 \alpha$, where α is the angle of the proton in the θ^+ centre-of-mass system. The associated systematic uncertainty is found to be 6%. Limited Monte Carlo statistics introduces an additional uncertainty of 5%. The sum in quadrature of these contributions yields a total systematic uncertainty of 16%. Including this uncertainty in the determination of the number of θ^+ pentaquark per two-photon hadronic event gives

$$\langle n_{\theta^+} \rangle < 4.7 \times 10^{-3}$$

at 95% confidence level. This result is about four times greater than the mean $\Xi^*(1530)$ multiplicity: a baryon with almost the same mass. This difference is mainly due to the stringent cuts applied to proton selection, resulting in a smaller selection efficiency than that of the $\Xi^*(1530)$ baryon, as well as the low branching ratio $\theta^+ \to pK_S^0$, considered as half of that of the decay $\Xi^*(1530) \to \Lambda\pi^-\pi^+ \to p\pi^-\pi^-\pi^+$.

Using the two-photon cross-section for $W_{\gamma\gamma} > 5$ GeV, $\sigma_{\gamma\gamma} = 397$ nb [27], a 95% C.L. upper limit on the cross section $\gamma\gamma \to \theta^+ X$ of 1.8 nb is obtained. This result is comparable to the upper limit obtained by the photoproduction experiment in the reaction $\gamma p \to \overline{K}^0 \theta^+$ [11].

As a cross check, several subsets of the selected pK_S^0 samples were investigated using tighter selection criteria. The K_S^0 selection interval was reduced to ± 10 MeV, the DCA of proton and antiprotons candidates was required to be less than 3 mm or secondary vertices compatible with the Λ mass hypothesis were rejected. Since strangeness is a conserved quantity in strong interactions, the presence of an additional kaon was also required. No significant θ^+ signal was observed in any of these samples.

8 Conclusion

The production of Λ, Ξ^- and $\Xi^*(1530)$ baryons in two-photon collisions is studied in the range 0.4 GeV $< p_t < 2.5$ GeV, $|\eta| < 1.2$ and $W_{\gamma\gamma} > 5$ GeV. The shape of the differential cross section for Λ and Ξ^- production is relatively well reproduced by the PYTHIA and PHOJET Monte Carlo programs using parameters tuned at $\sqrt{s} = m_Z$ although a better agreement can be obtained for Λ by increasing the width in the gaussian p_t distribution for primary hadrons. The mean numbers of Λ, Ξ^- and $\Xi^*(1530)$ baryons per hadronic two-photon event are found to be slightly below the PYTHIA and PHOJET predictions but overall agreement with the thermodynamical model is observed. The comparison between measurements obtained in two-photon events and e^+e^- annihilation processes provides evidence for the universality of fragmentation functions in both reactions.

Finally, a search for the pentaquark $\theta^+(1540)$ through the decay $\theta^+ \to pK_S^0$ for $W_{\gamma\gamma} > 5$ GeV is presented. No evidence for θ^+ production is found and a 95% confidence level upper limit on the mean number of θ^+ per two-photon hadronic event at a level of four times the observed rate for the $\Xi^*(1530)$ baryon is derived.

References

[1] B. Andersson *et al.*, Phys. Rep. **97** (1983) 31.

[2] B. Andersson, G. Gustafson and T. Sjöstrand, Phys. Scripta **32** (1985) 574.

[3] F. Becattini and L. Ferroni, Eur. Phys. J. C **35** (2004) 243;
    F. Becattini and L. Ferroni, Eur. Phys. J. C **38** (2004) 225; and references therein.

[4] L3 Collab., P. Achard *et al.*, Phys. Lett. **B 524** (2002) 44.

[5] L3 Collab., P. Achard *et al.*, Phys. Lett. **B 586** (2004) 140.

[6] L3 Collab., B. Adeva *et al.*, Nucl. Instr. Meth. **A 289** (1990) 35;
    L3 Collab., O. Adriani *et al.*, Phys. Rept. **236** (1993) 1;
    M. Chemarin *et al.*, Nucl. Instr. Meth. **A 349** (1994) 345;
    M. Acciarri *et al.*, Nucl. Instr. Meth. **A 351** (1994) 300;
    I. C. Brock *et al.*, Nucl. Instr. Meth. **A 381** (1996) 236;
    A. Adam *et al.*, Nucl. Instr. Meth. **A 383** (1996) 342.

[7] Particle Data Group, S. Eidelman *et al.*, Phys. Lett. **B 592** (2004) 1.

[8] TOPAZ Collab., R. Enomoto *et al.*, Phys. Lett. **B 347** (1995) 179.

[9] LEPS Collab., T. Nakano *et al.*, Phys. Rev. Lett. **91** (2003) 012002.

[10] WA89 Collab., M. I. Adamovich *et al.*, Phys. Rev. **C 72** (2005) 055201, and references therein.

[11] CLAS Collab., R. De Vita *et al.*, hep-ex/0606062, and references therein.

[12] PYTHIA version 5.722 and JETSET version 7.409 are used with default options;
    T. Sjöstrand, Comp. Phys. Comm. **82** (1994) 74.

[13] PHOJET version 1.05c is used with default options;
    R. Engel, Z. Phys. **C 66** (1995) 203;
    R. Engel and J. Ranft, Phys. Rev. **D 54** (1996) 4244.

[14] G. A. Schuler and T. Sjöstrand, Z. Phys. **C 68** (1995) 607.

[15] V. M. Budnev *et al.*, Phys. Rep. **15** (1974) 181.

[16] A. Capella *et al.*, Phys. Rep. **236** (1994) 225.

[17] M. Glück, E. Reya and A. Vogt, Phys. Rev. **D 45** (1992) 3986; Phys. Rev. **D46** (1992) 1973.

[18] L3 Collab., P. Achard *et al.*, Phys. Rept. **399** (2004) 71.

[19] KK2f version 4.12 is used;
    S. Jadach, B. F. L. Ward and Z. Wąs, Comp. Phys. Comm. **130** (2000) 260.

[20] KORALZ version 4.04 is used;
    S. Jadach, B. F. L. Ward and Z. Wąs, Comp. Phys. Comm. **79** (1994) 503.

[21] KORALW version 1.33 is used;
M. Skrzypek *et al.*, Comp. Phys. Comm. **94** (1996) 216.

[22] DIAG36 version 1.0 is used;
F. A. Berends, P. H. Daverfeldt and R. Kleiss, Nucl. Phys. **B 253** (1985) 441.

[23] GEANT version 3.15 is used;
R. Brun *et al.*, CERN report CERN DD/EE/84-1 (1984), revised 1987.

[24] H. Fesefeldt, RWTH Aachen report PITHA 85/2 (1985).

[25] P. Béné *et al.*, Nucl. Inst. Meth. **A 306** (1991) 150;
D. Haas *et al.*, Nucl. Inst. Meth. **A 420** (1991) 101.

[26] R. Bizzarri *et al.*, Nucl. Instr. Meth. **A 283** (1989) 799.

[27] L3 Collab., M. Acciarri *et al.*, Phys. Lett. **B 519** (2001) 33.

[28] R. D. Field and R. P. Feynman, Nucl Phys **B 136** (1978) 1.

[29] F. Becattini and G. Passaleva, Eur. Phys. J. C **23** (2002) 551.

[30] P. V. Chliapnikov and V. A. Uvarov, Phys. Lett. **B 345** (1995) 313.

The L3 Collaboration:

P.Achard,[20] O.Adriani,[17] M.Aguilar-Benitez,[25] J.Alcaraz,[25] G.Alemanni,[23] J.Allaby,[18] A.Aloisio,[29] M.G.Alviggi,[29] H.Anderhub,[49] V.P.Andreev,[6,34] F.Anselmo,[8] A.Arefiev,[28] T.Azemoon,[3] T.Aziz,[9] P.Bagnaia,[39] A.Bajo,[25] G.Baksay,[26] L.Baksay,[26] S.V.Baldew,[2] S.Banerjee,[9] Sw.Banerjee,[4] A.Barczyk,[49,47] R.Barillère,[18] P.Bartalini,[23] M.Basile,[8] N.Batalova,[46] R.Battiston,[33] A.Bay,[23] F.Becattini,[17] U.Becker,[13] F.Behner,[49] L.Bellucci,[17] R.Berbeco,[3] J.Berdugo,[25] P.Berges,[13] B.Bertucci,[33] B.L.Betev,[49] M.Biasini,[33] M.Biglietti,[29] A.Biland,[49] J.J.Blaising,[4] S.C.Blyth,[35] G.J.Bobbink,[2] A.Böhm,[1] L.Boldizsar,[12] B.Borgia,[39] S.Bottai,[17] D.Bourilkov,[49] M.Bourquin,[20] S.Braccini,[20] J.G.Branson,[41] F.Brochu,[4] J.D.Burger,[13] W.J.Burger,[33] X.D.Cai,[13] M.Capell,[13] G.Cara Romeo,[8] G.Carlino,[29] A.Cartacci,[17] J.Casaus,[25] F.Cavallari,[39] N.Cavallo,[36] C.Cecchi,[33] M.Cerrada,[25] M.Chamizo,[20] Y.H.Chang,[44] M.Chemarin,[24] A.Chen,[44] G.Chen,[7] G.M.Chen,[7] H.F.Chen,[22] H.S.Chen,[7] G.Chiefari,[29] L.Cifarelli,[40] F.Cindolo,[8] I.Clare,[13] R.Clare,[38] G.Coignet,[4] N.Colino,[25] S.Costantini,[39] B.de la Cruz,[25] S.Cucciarelli,[33] R.de Asmundis,[29] P.Déglon,[20] J.Debreczeni,[12] A.Degré,[4] K.Dehmelt,[26] K.Deiters,[47] D.della Volpe,[29] E.Delmeire,[20] P.Denes,[37] F.DeNotaristefani,[39] A.De Salvo,[49] M.Diemoz,[39] M.Dierckxsens,[2] C.Dionisi,[39] M.Dittmar,[49] A.Doria,[29] M.T.Dova,[10,♯] D.Duchesneau,[4] M.Duda,[1] B.Echenard,[20] A.Eline,[18] A.El Hage,[1] H.El Mamouni,[24] A.Engler,[35] F.J.Eppling,[13] P.Extermann,[20] M.A.Falagan,[25] S.Falciano,[39] A.Favara,[32] J.Fay,[24] O.Fedin,[34] M.Felcini,[49] T.Ferguson,[35] H.Fesefeldt,[1] E.Fiandrini,[33] J.H.Field,[20] F.Filthaut,[31] P.H.Fisher,[13] W.Fisher,[37] G.Forconi,[13] K.Freudenreich,[49] C.Furetta,[27] Yu.Galaktionov,[28,13] S.N.Ganguli,[9] P.Garcia-Abia,[25] M.Gataullin,[32] S.Gentile,[39] S.Giagu,[39] Z.F.Gong,[22] G.Grenier,[24] O.Grimm,[49] M.W.Gruenewald,[16] V.K.Gupta,[37] A.Gurtu,[9] L.J.Gutay,[46] D.Haas,[5] D.Hatzifotiadou,[8] T.Hebbeker,[1] A.Hervé,[18] J.Hirschfelder,[35] H.Hofer,[49] M.Hohlmann,[26] G.Holzner,[49] S.R.Hou,[44] B.N.Jin,[7] P.Jindal,[14] L.W.Jones,[3] P.de Jong,[2] I.Josa-Mutuberría,[25] M.Kaur,[14] M.N.Kienzle-Focacci,[20] J.K.Kim,[43] J.Kirkby,[18] W.Kittel,[31] A.Klimentov,[13,28] A.C.König,[31] M.Kopal,[46] V.Koutsenko,[13,28] M.Kräber,[49] R.W.Kraemer,[35] A.Krüger,[48] A.Kunin,[13] P.Ladron de Guevara,[25] I.Laktineh,[24] G.Landi,[17] M.Lebeau,[18] A.Lebedev,[13] P.Lebrun,[24] P.Lecomte,[49] P.Lecoq,[18] P.Le Coultre,[49] J.M.Le Goff,[18] R.Leiste,[48] M.Levtchenko,[27] P.Levtchenko,[34] C.Li,[22] S.Likhoded,[48] C.H.Lin,[44] W.T.Lin,[44] F.L.Linde,[2] L.Lista,[29] Z.A.Liu,[7] W.Lohmann,[48] E.Longo,[39] Y.S.Lu,[7] C.Luci,[39] L.Luminari,[39] W.Lustermann,[49] W.G.Ma,[22] L.Malgeri,[18] A.Malinin,[28] C.Maña,[25] J.Mans,[37] J.P.Martin,[24] F.Marzano,[39] K.Mazumdar,[9] R.R.McNeil,[6] S.Mele,[18,29] L.Merola,[29] M.Meschini,[17] W.J.Metzger,[31] A.Mihul,[11] H.Milcent,[18] G.Mirabelli,[39] J.Mnich,[1] G.B.Mohanty,[9] G.S.Muanza,[24] A.J.M.Muijs,[2] M.Musy,[39] S.Nagy,[15] S.Natale,[20] M.Napolitano,[29] F.Nessi-Tedaldi,[49] H.Newman,[32] A.Nisati,[39] T.Novak,[31] H.Nowak,[48] R.Ofierzynski,[49] G.Organtini,[39] I.Pal,[46] C.Palomares,[25] P.Paolucci,[29] R.Paramatti,[39] G.Passaleva,[17] S.Patricelli,[29] T.Paul,[10] M.Pauluzzi,[33] C.Paus,[13] F.Pauss,[49] M.Pedace,[39] S.Pensotti,[27] D.Perret-Gallix,[4] D.Piccolo,[29] F.Pierella,[8] M.Pieri,[41] M.Pioppi,[33] P.A.Piroué,[37] E.Pistolesi,[27] V.Plyaskin,[28] M.Pohl,[20] V.Pojidaev,[17] J.Pothier,[18] D.Prokofiev,[34] G.Rahal-Callot,[49] M.A.Rahaman,[9] P.Raics,[15] N.Raja,[9] R.Ramelli,[49] P.G.Rancoita,[27] R.Ranieri,[17] A.Raspereza,[48] P.Razis,[30] S.Rembeczki,[26] D.Ren,[49] M.Rescigno,[39] S.Reucroft,[10] S.Riemann,[48] K.Riles,[3] B.P.Roe,[3] L.Romero,[25] A.Rosca,[48] C.Rosemann,[1] C.Rosenbleck,[1] S.Rosier-Lees,[4] S.Roth,[1] J.A.Rubio,[18] G.Ruggiero,[17] H.Rykaczewski,[49] A.Sakharov,[49] S.Saremi,[6] S.Sarkar,[39] J.Salicio,[18] E.Sanchez,[25] C.Schäfer,[18] V.Schegelsky,[34] H.Schopper,[21] D.J.Schotanus,[31] C.Sciacca,[29] L.Servoli,[33] S.Shevchenko,[32] N.Shivarov,[42] V.Shoutko,[13] E.Shumilov,[28] A.Shvorob,[32] D.Son,[43] C.Souga,[24] P.Spillantini,[17] M.Steuer,[13] D.P.Stickland,[37] B.Stoyanov,[42] A.Straessner,[20] K.Sudhakar,[9] G.Sultanov,[42] L.Z.Sun,[22] S.Sushkov,[1] H.Suter,[49] J.D.Swain,[10] Z.Szillasi,[26,¶] X.W.Tang,[7] P.Tarjan,[15] L.Tauscher,[5] L.Taylor,[10] B.Tellili,[24] D.Teyssier,[24] C.Timmermans,[31] Samuel C.C.Ting,[13] S.M.Ting,[13] S.C.Tonwar,[9] J.Tóth,[12] C.Tully,[37] K.L.Tung,[7] J.Ulbricht,[49] E.Valente,[39] R.T.Van de Walle,[31] R.Vasquez,[46] G.Vesztergombi,[12] I.Vetlitsky,[28] G.Viertel,[49] M.Vivargent,[4] S.Vlachos,[5] I.Vodopianov,[26] H.Vogel,[35] H.Vogt,[48] I.Vorobiev,[35,28] A.A.Vorobyov,[34] M.Wadhwa,[5] Q.Wang,[31] X.L.Wang,[22] Z.M.Wang,[22] M.Weber,[18] S.Wynhoff,[37,†] L.Xia,[32] Z.Z.Xu,[22] J.Yamamoto,[3] B.Z.Yang,[22] C.G.Yang,[7] H.J.Yang,[3] M.Yang,[7] S.C.Yeh,[45] An.Zalite,[34] Yu.Zalite,[34] Z.P.Zhang,[22] J.Zhao,[22] G.Y.Zhu,[7] R.Y.Zhu,[32] H.L.Zhuang,[7] A.Zichichi,[8,18,19] B.Zimmermann,[49] M.Zöller.[1]

1 III. Physikalisches Institut, RWTH, D-52056 Aachen, Germany[§]
2 National Institute for High Energy Physics, NIKHEF, and University of Amsterdam, NL-1009 DB Amsterdam, The Netherlands
3 University of Michigan, Ann Arbor, MI 48109, USA
4 Laboratoire d'Annecy-le-Vieux de Physique des Particules, LAPP,IN2P3-CNRS, BP 110, F-74941 Annecy-le-Vieux CEDEX, France
5 Institute of Physics, University of Basel, CH-4056 Basel, Switzerland
6 Louisiana State University, Baton Rouge, LA 70803, USA
7 Institute of High Energy Physics, IHEP, 100039 Beijing, China[△]
8 University of Bologna and INFN-Sezione di Bologna, I-40126 Bologna, Italy
9 Tata Institute of Fundamental Research, Mumbai (Bombay) 400 005, India
10 Northeastern University, Boston, MA 02115, USA
11 Institute of Atomic Physics and University of Bucharest, R-76900 Bucharest, Romania
12 Central Research Institute for Physics of the Hungarian Academy of Sciences, H-1525 Budapest 114, Hungary[‡]
13 Massachusetts Institute of Technology, Cambridge, MA 02139, USA
14 Panjab University, Chandigarh 160 014, India
15 KLTE-ATOMKI, H-4010 Debrecen, Hungary[¶]
16 UCD School of Physics, University College Dublin, Belfield, Dublin 4, Ireland
17 INFN Sezione di Firenze and University of Florence, I-50125 Florence, Italy
18 European Laboratory for Particle Physics, CERN, CH-1211 Geneva 23, Switzerland
19 World Laboratory, FBLJA Project, CH-1211 Geneva 23, Switzerland
20 University of Geneva, CH-1211 Geneva 4, Switzerland
21 University of Hamburg, D-22761 Hamburg, Germany
22 Chinese University of Science and Technology, USTC, Hefei, Anhui 230 029, China[△]
23 University of Lausanne, CH-1015 Lausanne, Switzerland
24 Institut de Physique Nucléaire de Lyon, IN2P3-CNRS,Université Claude Bernard, F-69622 Villeurbanne, France
25 Centro de Investigaciones Energéticas, Medioambientales y Tecnológicas, CIEMAT, E-28040 Madrid, Spain[♭]
26 Florida Institute of Technology, Melbourne, FL 32901, USA
27 INFN-Sezione di Milano, I-20133 Milan, Italy
28 Institute of Theoretical and Experimental Physics, ITEP, Moscow, Russia
29 INFN-Sezione di Napoli and University of Naples, I-80125 Naples, Italy
30 Department of Physics, University of Cyprus, Nicosia, Cyprus
31 Radboud University and NIKHEF, NL-6525 ED Nijmegen, The Netherlands
32 California Institute of Technology, Pasadena, CA 91125, USA
33 INFN-Sezione di Perugia and Università Degli Studi di Perugia, I-06100 Perugia, Italy
34 Nuclear Physics Institute, St. Petersburg, Russia
35 Carnegie Mellon University, Pittsburgh, PA 15213, USA
36 INFN-Sezione di Napoli and University of Potenza, I-85100 Potenza, Italy
37 Princeton University, Princeton, NJ 08544, USA
38 University of Californa, Riverside, CA 92521, USA
39 INFN-Sezione di Roma and University of Rome, "La Sapienza", I-00185 Rome, Italy
40 University and INFN, Salerno, I-84100 Salerno, Italy
41 University of California, San Diego, CA 92093, USA
42 Bulgarian Academy of Sciences, Central Lab. of Mechatronics and Instrumentation, BU-1113 Sofia, Bulgaria
43 The Center for High Energy Physics, Kyungpook National University, 702-701 Taegu, Republic of Korea
44 National Central University, Chung-Li, Taiwan, China
45 Department of Physics, National Tsing Hua University, Taiwan, China
46 Purdue University, West Lafayette, IN 47907, USA
47 Paul Scherrer Institut, PSI, CH-5232 Villigen, Switzerland
48 DESY, D-15738 Zeuthen, Germany
49 Eidgenössische Technische Hochschule, ETH Zürich, CH-8093 Zürich, Switzerland

p_t (GeV)	$\langle p_t \rangle$ (GeV)	$\langle p_t^2 \rangle$ (GeV^2)	Number of baryons	Efficiency (%)	$\mathrm{d}\sigma/\mathrm{d}p_t$ (pb/ GeV)	$\mathrm{d}\sigma/\mathrm{d}p_t^2$ (pb/ GeV^2)
Λ baryon
0.4−0.6	0.50	0.25	3412 ± 71	10.2 ± 0.1	$273.1 \pm 5.7 \pm 35.7$	$273.1 \pm 5.7 \pm 35.7$
0.6−0.8	0.69	0.48	4408 ± 85	13.7 ± 0.1	$264.1 \pm 5.1 \pm 29.1$	$188.7 \pm 3.6 \pm 20.8$
0.8−1.0	0.89	0.79	3420 ± 81	15.3 ± 0.2	$183.3 \pm 4.4 \pm 15.3$	$101.9 \pm 2.4 \pm 8.5$
1.0−1.3	1.12	1.27	3201 ± 87	16.8 ± 0.2	$103.9 \pm 2.8 \pm 7.8$	$45.2 \pm 1.2 \pm 3.4$
1.3−1.6	1.43	2.05	1222 ± 55	17.7 ± 0.4	$37.8 \pm 1.7 \pm 3.1$	$13.0 \pm 0.6 \pm 1.1$
1.6−2.0	1.77	3.14	578 ± 41	15.9 ± 0.6	$15.0 \pm 1.1 \pm 1.4$	$4.2 \pm 0.3 \pm 0.4$
2.0−2.5	2.21	4.92	292 ± 25	17.2 ± 1.3	$5.6 \pm 0.5 \pm 1.2$	$1.2 \pm 0.1 \pm 0.3$
Ξ^- baryon
0.4−0.7	0.55	0.31	70 ± 10	3.4 ± 0.2	$11.3 \pm 1.7 \pm 1.7$	$10.3 \pm 1.5 \pm 1.6$
0.7−1.0	0.83	0.70	113 ± 12	7.1 ± 0.3	$8.7 \pm 1.2 \pm 1.2$	$5.1 \pm 0.6 \pm 0.7$
1.0−1.3	1.13	1.27	83 ± 12	9.7 ± 0.8	$4.7 \pm 0.8 \pm 0.8$	$2.0 \pm 0.3 \pm 0.3$
1.3−2.5	1.67	2.88	94 ± 19	8.8 ± 0.9	$1.5 \pm 0.3 \pm 0.3$	$0.4 \pm 0.1 \pm 0.1$
$\Xi^*(1530)$ baryon
0.4−2.5	0.82	0.84	56 ± 13	3.8 ± 0.6	$1.4 \pm 0.3 \pm 0.5$	$0.5 \pm 0.1 \pm 0.2$

Table 1: The average transverse momentum $\langle p_t \rangle$, the average transverse momentum squared $\langle p_t^2 \rangle$, the number of baryons estimated by the fits to the Λ, Ξ^- and $\Xi^*(1530)$ mass spectra, the detection efficiency and the differential cross sections $\mathrm{d}\sigma/\mathrm{d}p_t$ and $\mathrm{d}\sigma/\mathrm{d}p_t^2$ for inclusive Λ, Ξ^- and $\Xi^*(1530)$ production as a function of p_t for $|\eta| < 1.2$. The first uncertainty on the cross sections is statistical and the second systematic.

$|\eta|$	$\langle |\eta| \rangle$	Number of baryons	Efficiency (%)	$\mathrm{d}\sigma/\mathrm{d}|\eta|$ (pb)
Λ baryon \quad 0.4 GeV $< p_t <$ 1.0 GeV
0.0−0.3	0.15	2953 ± 72	13.8 ± 0.2	$58.6 \pm 1.4 \pm 3.4$
0.3−0.6	0.45	2742 ± 63	13.4 ± 0.2	$56.1 \pm 1.3 \pm 3.2$
0.6−0.9	0.75	2904 ± 70	13.0 ± 0.2	$61.0 \pm 1.5 \pm 4.1$
0.9−1.2	1.05	2774 ± 89	11.1 ± 0.1	$68.0 \pm 2.2 \pm 8.4$
Λ baryon \quad 1.0 GeV $< p_t <$ 2.5 GeV
0.0−0.3	0.15	1458 ± 60	18.8 ± 0.5	$21.2 \pm 0.9 \pm 1.6$
0.3−0.6	0.45	1411 ± 62	18.2 ± 0.4	$21.2 \pm 0.9 \pm 1.6$
0.6−0.9	0.75	1480 ± 62	19.3 ± 0.5	$20.9 \pm 0.9 \pm 1.6$
0.9−1.2	1.05	1007 ± 62	14.3 ± 0.4	$19.3 \pm 1.2 \pm 2.7$
Ξ^- baryon \quad 0.4 GeV $< p_t <$ 2.5 GeV
0.0−0.4	0.20	110 ± 14	6.7 ± 0.3	$6.9 \pm 0.9 \pm 1.0$
0.4−0.8	0.60	114 ± 13	6.1 ± 0.2	$8.0 \pm 1.0 \pm 1.0$
0.8−1.2	1.01	109 ± 15	5.5 ± 0.2	$7.6 \pm 1.1 \pm 1.2$

Table 2: The average pseudo-rapidity $\langle |\eta| \rangle$, the number of baryons estimated by the fits to the Λ and Ξ^- mass spectra, the detection efficiency and the differential cross sections $\mathrm{d}\sigma/\mathrm{d}|\eta|$ for inclusive Λ and Ξ^- production as a function of $|\eta|$. The first uncertainty on the cross sections is statistical and the second systematic.

	Data	PYTHIA	PHOJET
	0.4 GeV $< p_t <$ 2.5 GeV, $|\eta| < 1.2$ and $W_{\gamma\gamma} > 5$ GeV		
$\langle n_\Lambda \rangle$	$(1.6 \pm 0.1) \times 10^{-2}$	$(1.43 \pm 0.01) \times 10^{-2}$	$(1.80 \pm 0.01) \times 10^{-2}$
$\langle n_{\Xi^-} \rangle$	$(7.6 \pm 1.0) \times 10^{-4}$	$(8.61 \pm 0.11) \times 10^{-4}$	$(11.5 \pm 0.10) \times 10^{-4}$
$\langle n_{\Xi^*(1530)} \rangle$	$(2.3 \pm 1.0) \times 10^{-4}$	$(1.37 \pm 0.04) \times 10^{-4}$	$(1.91 \pm 0.03) \times 10^{-4}$

	Data	PYTHIA	PHOJET
	$W_{\gamma\gamma} > 5$ GeV		
$\langle n_\Lambda \rangle$	$(7.6 \pm 0.8) \times 10^{-2}$	$(8.51 \pm 0.01) \times 10^{-2}$	$(1.11 \pm 0.01) \times 10^{-1}$
$\langle n_{\Xi^-} \rangle$	$(3.7 \pm 0.5) \times 10^{-3}$	$(5.17 \pm 0.02) \times 10^{-3}$	$(7.29 \pm 0.09) \times 10^{-3}$
$\langle n_{\Xi^*(1530)} \rangle$	$(11.8 \pm 5.2) \times 10^{-4}$	$(8.65 \pm 0.09) \times 10^{-4}$	$(12.4 \pm 0.10) \times 10^{-3}$

Table 3: The mean number of Λ, Ξ^- and $\Xi^*(1530)$ baryons per hadronic two-photon event for the measured p_t and $|\eta|$ phase-space (top) and its extrapolation (bottom) to the full p_t and $|\eta|$ range. The uncertainty on data includes both the statistical and systematic contributions whereas the uncertainty on the Monte Carlo predictions is statistical.

p_t (GeV)	Selection criteria	Background subtraction	Monte Carlo statistics	Monte Carlo modelling	Total
Λ baryon					
0.4−0.6	4.2	12.1	0.9	1.4	13.1
0.6−0.8	4.2	9.8	0.9	1.6	11.0
0.8−1.0	4.2	6.6	1.2	1.9	8.4
1.0−1.3	4.2	5.3	1.4	2.1	7.5
1.3−1.6	4.2	5.8	2.4	2.4	8.2
1.6−2.0	4.2	6.4	3.5	2.8	9.1
2.0−2.5	4.2	19.4	7.5	4.8	21.8
Ξ baryon					
0.4−0.7	10.3	8.7	5.8	3.1	15.1
0.7−1.0	10.3	7.5	4.8	2.4	14.0
1.0−1.3	10.3	9.1	8.3	3.3	16.5
1.3−2.5	10.3	12.3	10.4	6.3	19.5
$\Xi^*(1530)$ baryon					
0.4−2.5	19.2	24.6	16.5	13.6	37.9

Table 4: Systematic uncertainties in percent on the cross section of the $e^+e^- \rightarrow e^+e^-\Lambda X$, $e^+e^- \rightarrow e^+e^-\Xi^- X$ and $e^+e^- \rightarrow e^+e^-\Xi^*(1530)X$ processes due to selection criteria, background subtraction, limited Monte Carlo statistics, Monte Carlo modelling and trigger efficiency as a function of p_t for $|\eta| < 1.2$. The total systematic uncertainty, taken as the quadratic sum of the different contributions, includes a constant contribution of 2% due to the determination of the trigger efficiency.
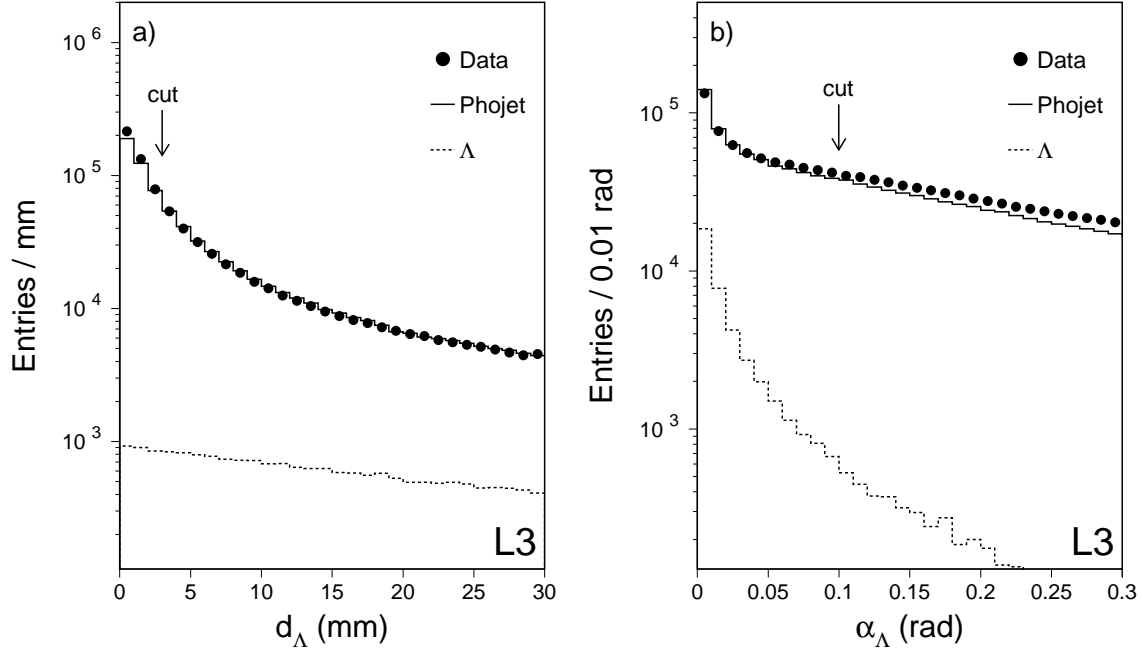
Figure 1: Distribution of the variables used to select secondary vertices from inclusive Λ production: a) the distance in the transverse plane between the secondary vertex and the e^+e^- interaction point, d_Λ, and b) the angle between the sum p_t vector of the two tracks and the direction in the transverse plane between the interaction point and the secondary vertex, α_Λ. All other secondary vertex selection criteria are applied. The predictions of the PHOJET Monte Carlo are shown as the solid lines and the contribution due to Λ baryons as the dashed lines. The Monte Carlo distributions are normalized to the data luminosity.
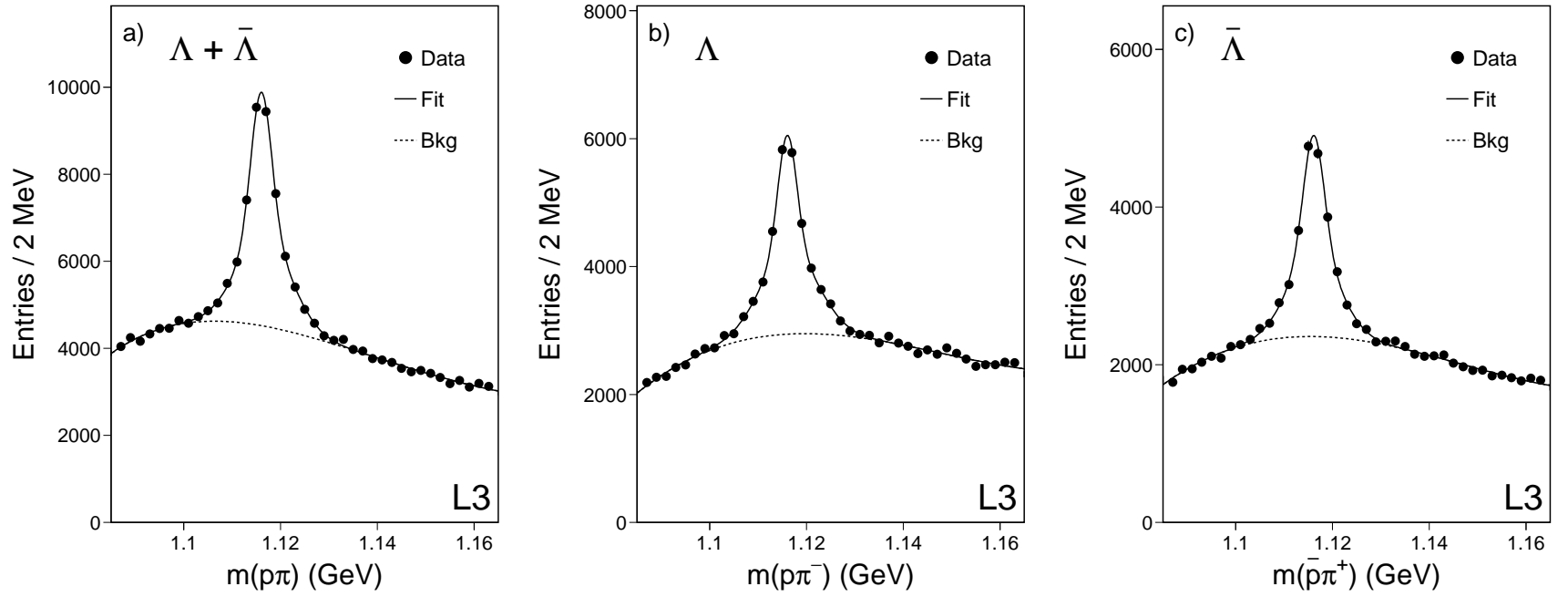
Figure 2: The mass of the pπ system for the inclusive Λ selection for a) Λ and $\overline{\Lambda}$ candidates, b) Λ candidates and c) $\overline{\Lambda}$ candidates. The signal is modelled with two Gaussians and the background by a fourth-order Chebyshev polynomial.
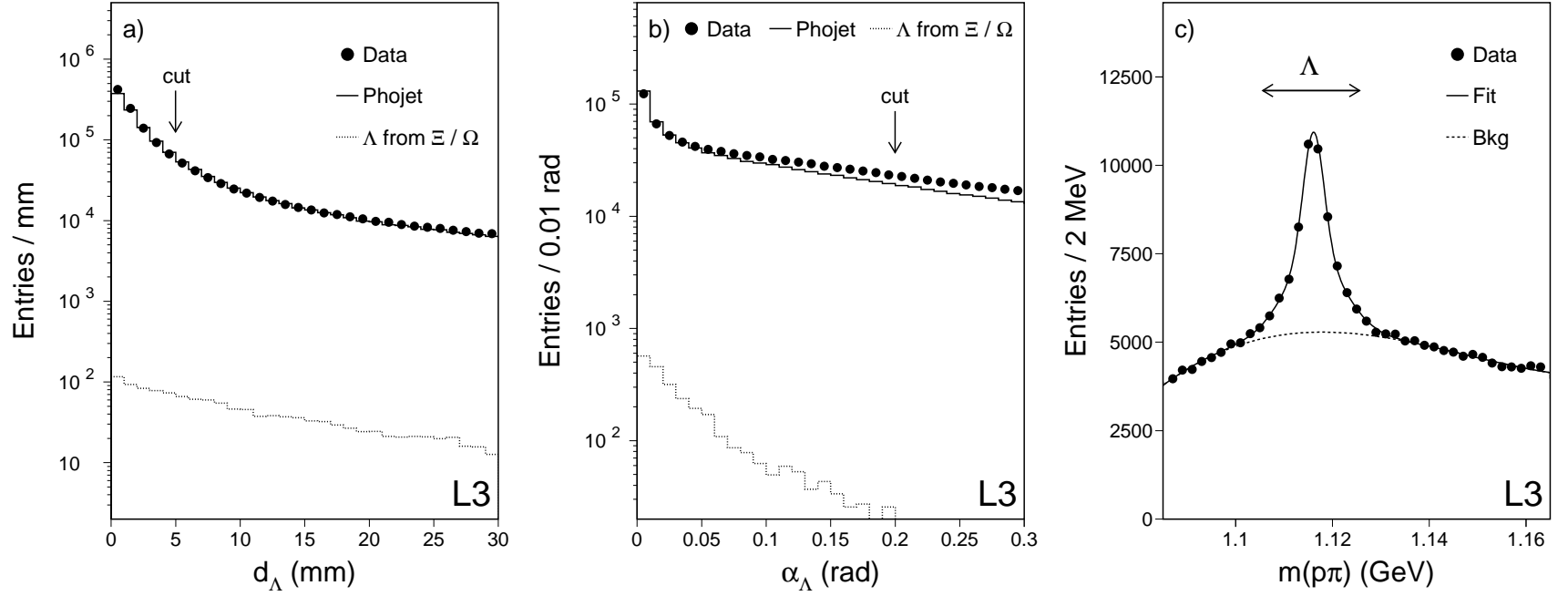
Figure 3: Distribution of the variables used to select secondary vertices from Λ produced in Ξ^- and Ω^- decays: a) the distance in the transverse plane between the secondary vertex and the e^+e^- interaction point, d_Λ, and b) the angle between the sum p_t vector of the two tracks and the direction in the transverse plane between the interaction point and the secondary vertex, α_Λ. All other secondary vertex selection criteria are applied. The predictions of the PHOJET Monte Carlo are shown as the full line and the contribution due to Λ baryons as the dashed line. c) The mass of the $p\pi$ system for Λ baryons produced in Ξ^- and Ω^- decays. The signal is modelled with two Gaussians and the background by a fourth-order Chebyshev polynomial. Only the combinations in the ± 10 MeV mass window indicated by the arrows are retained to reconstruct Ξ^- and Ω^- baryons. The Monte Carlo distributions are normalized to the data luminosity.
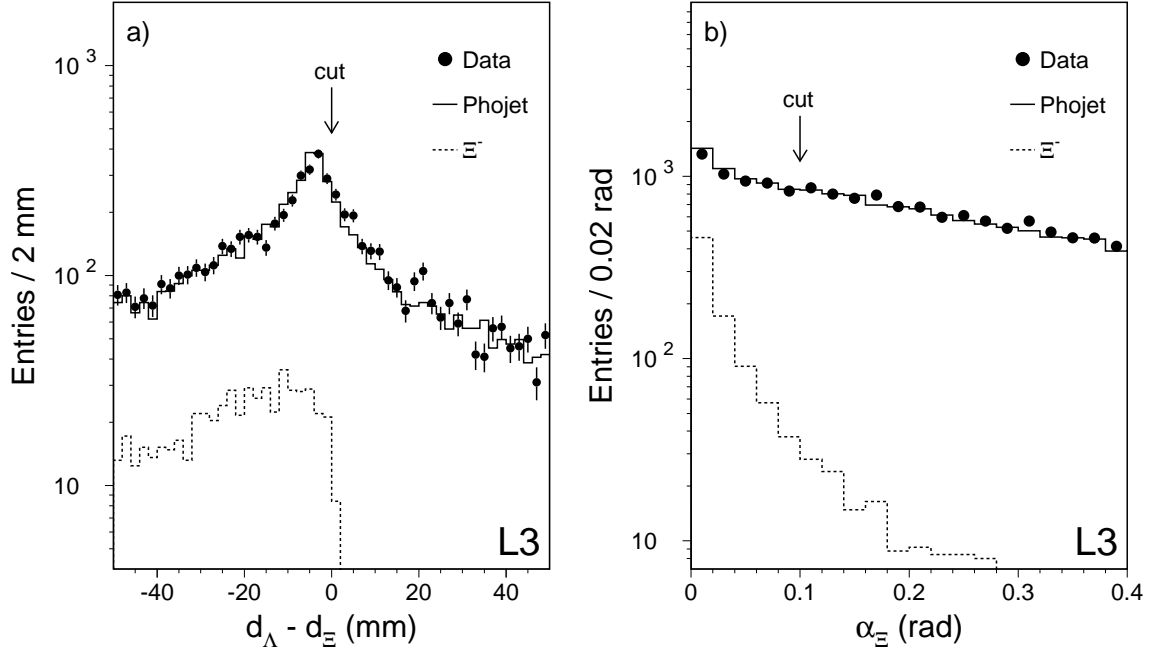
Figure 4: Distribution of the variables used for the selection of Ξ^- baryons: a) the difference $d_\Lambda - d_\Xi$ of the Λ and Ξ^- vertex distances from the interaction point and b) the angle α_Ξ between the p_t vector of the $\Lambda\pi$ combination and the direction in the transverse plane between the primary interaction point and the $\Lambda\pi$ vertex. In each plot, all other selection criteria are applied. The predictions of the PHOJET Monte Carlo are shown as the full line and the contribution due to Ξ^- baryons as the dashed line. The Monte Carlo distributions are normalized to the data luminosity.
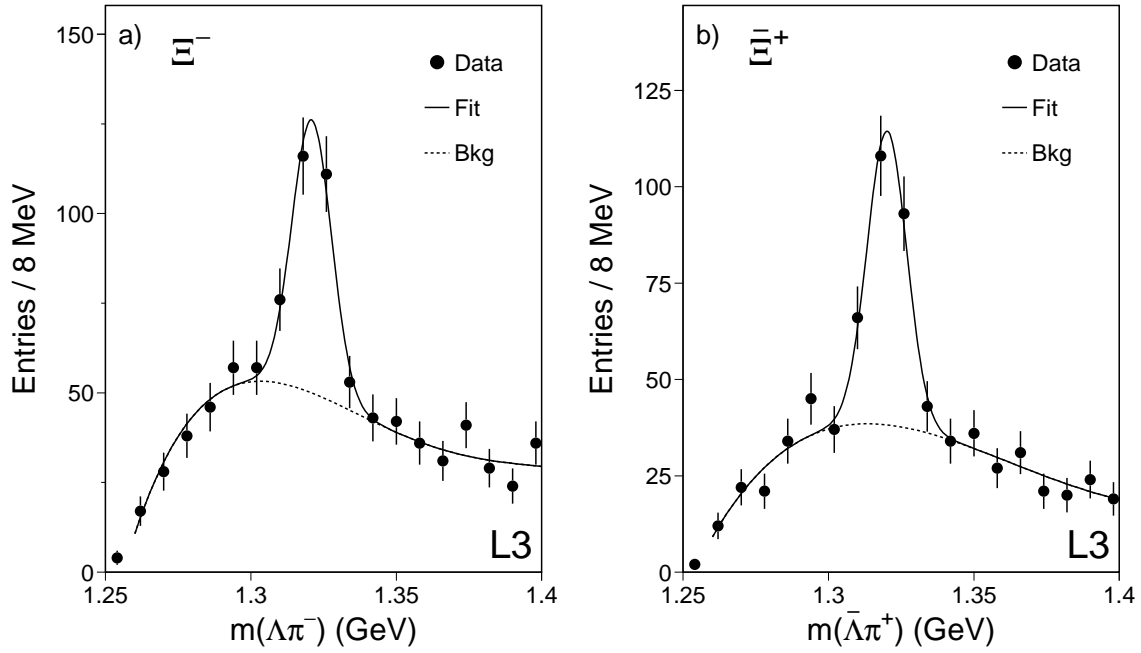
Figure 5: The mass spectrum of the $\Lambda\pi$ system for a) Ξ^- and b) $\overline{\Xi}^+$ candidates for 0.4 GeV < p_t < 2.5 GeV and $|\eta|$ < 1.2. The signal is modelled with a Gaussian and the background by a fourth order Chebyshev polynomial.
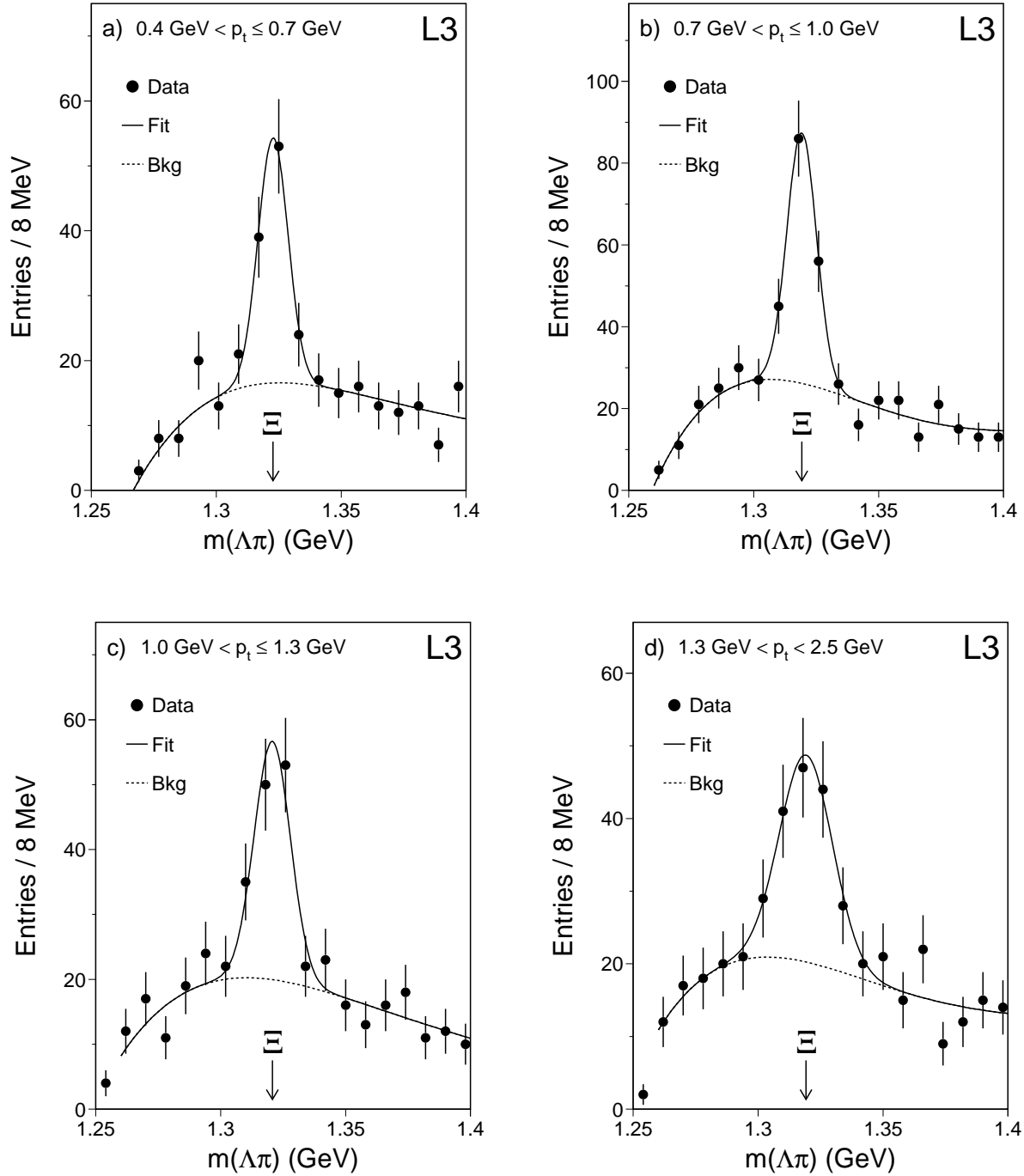
Figure 6: The mass of the $\Lambda\pi$ system for a) 0.4 GeV $< p_t \leq 0.7$ GeV, b) 0.7 GeV $< p_t \leq 1.0$ GeV, c) 1.0 GeV $< p_t < 1.3$ GeV and d) 1.3 GeV $< p_t < 2.5$ GeV. The signal is modelled with a Gaussian and the background by a fourth-order Chebyshev polynomial.
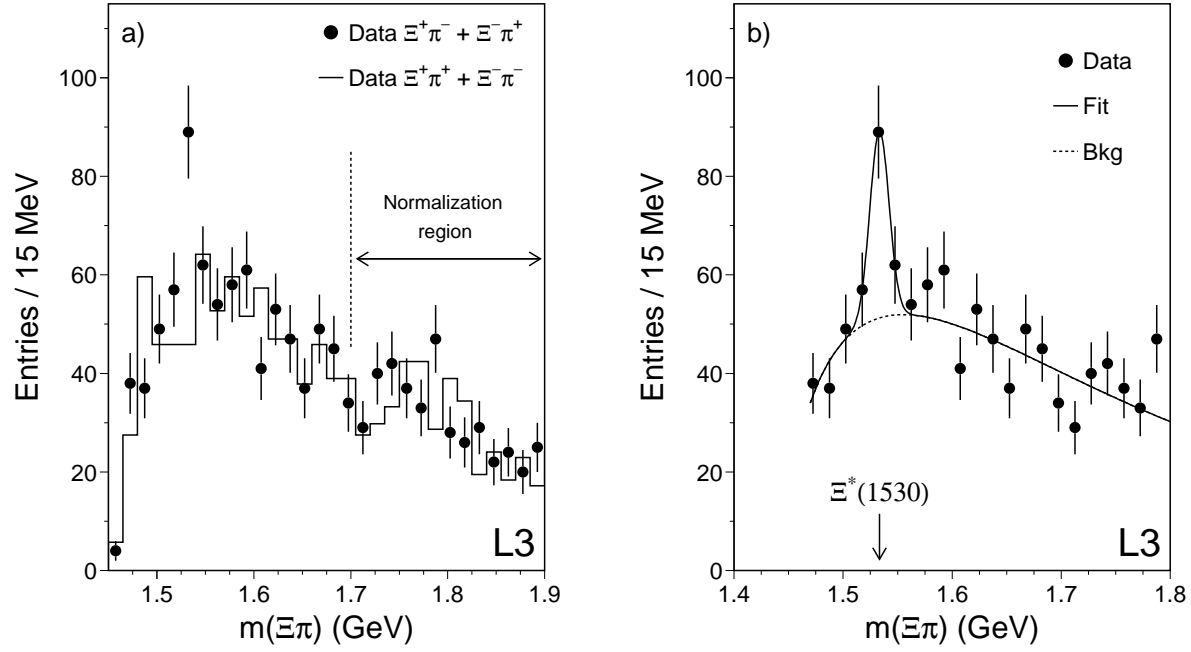
Figure 7: a) The mass of the $\Xi\pi$ system for opposite charge ($\Xi^-\pi^+$ and $\overline{\Xi}^+\pi^-$) and same-charge ($\Xi^-\pi^-$ and $\overline{\Xi}^+\pi^+$) combinations. The number of same-charge combinations is normalized to that of opposite-charge combinations in the region $m_{\Xi\pi} > 1.7$ GeV. A signal consistent with $\Xi^*(1530)$ production is observed. b) Fit to the mass spectrum of the opposite-charge combinations. The signal is modelled with a Gaussian and the background by a threshold function.
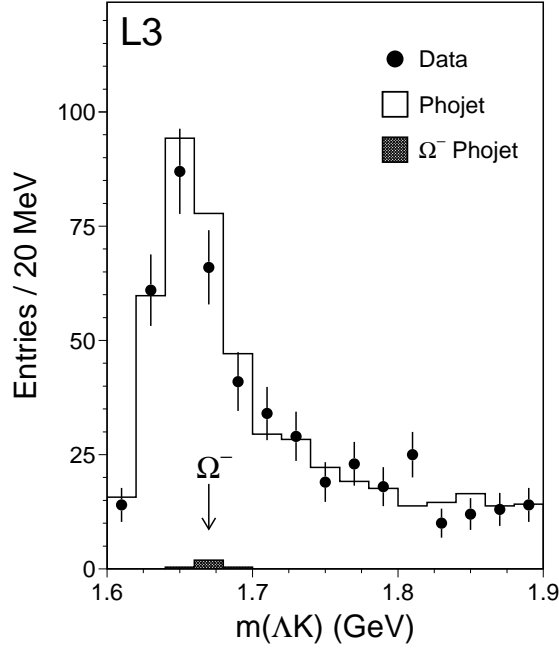
Figure 8: The mass of the ΛK system. No Ω^- signal is observed around the mass of 1.67 GeV. The predictions of the PHOJET Monte Carlo are shown as the full line and the contribution due to Ω^- baryons as the dashed histogram. The Monte Carlo distributions are normalized to the data luminosity.
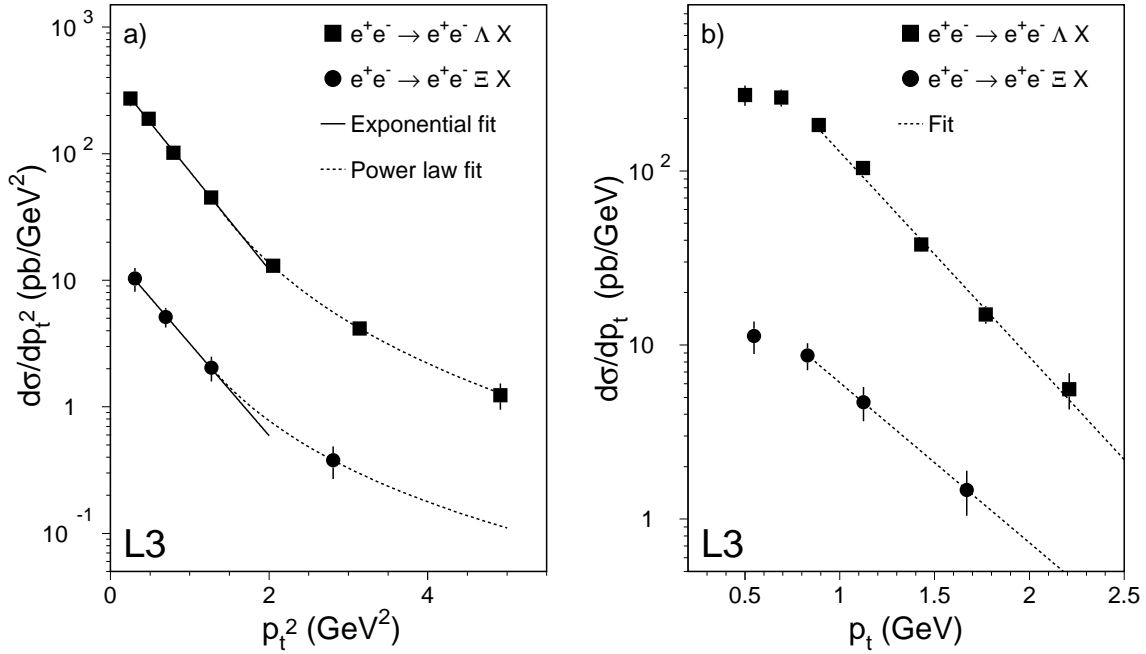
Figure 9: a) Differential cross sections $\mathrm{d}\sigma/\mathrm{d}p_t^2$ for the $e^+e^- \to e^+e^-\Lambda X$ and $e^+e^- \to e^+e^-\Xi^-X$ processes for $|\eta| < 1.2$. b) Differential cross sections $\mathrm{d}\sigma/\mathrm{d}p_t$ for the $e^+e^- \to e^+e^-\Lambda X$ and $e^+e^- \to e^+e^-\Xi^-X$ processes for $|\eta| < 1.2$. The various fits are described in the text.

24
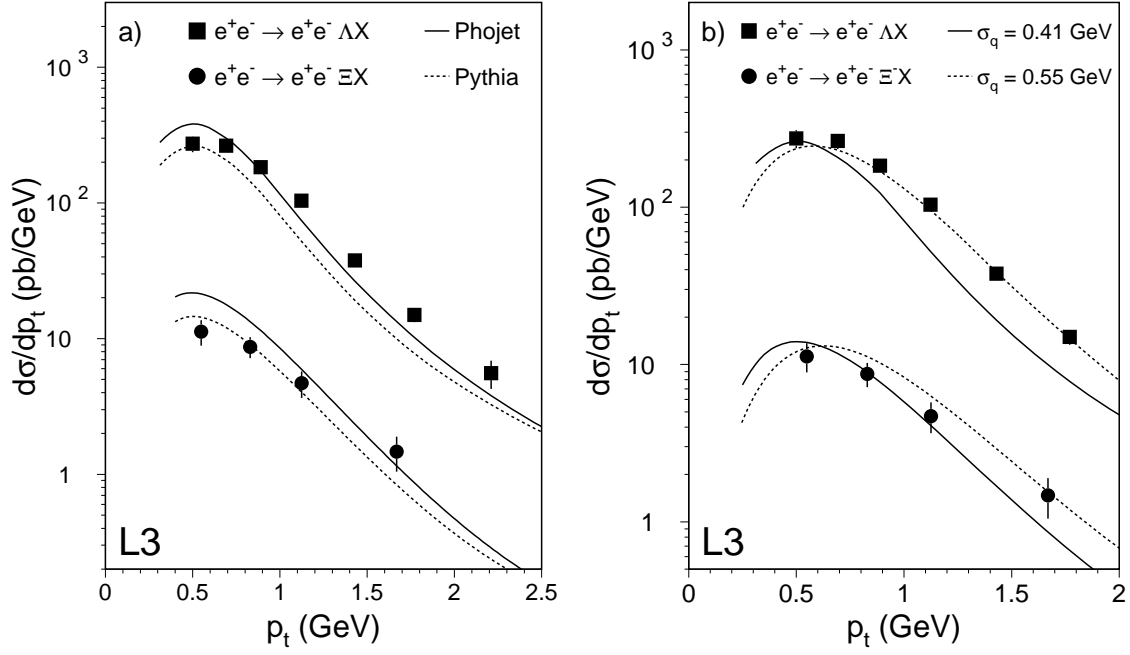
Figure 10: The differential cross section as a function of p_t for Λ and Ξ^- production for $|\eta| < 1.2$ compared with a) the predictions of the PHOJET and PYTHIA Monte Carlo, and b) the predictions of the PYTHIA Monte Carlo using the default value for the width σ_q in the Gaussian p_t distribution on primary hadrons $\sigma_q = 0.411$ GeV as well as the adjusted value $\sigma_q = 0.55$ GeV.
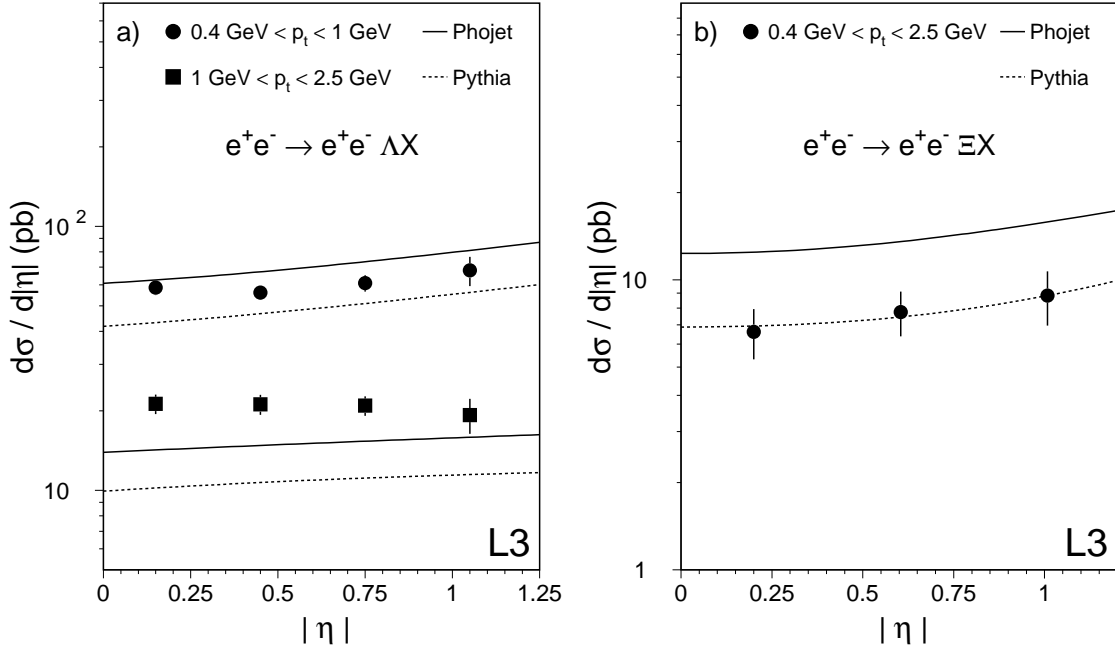
Figure 11: The differential cross section as a function of $|\eta|$ for a) inclusive Λ production for 0.4 GeV $< p_t < 1.0$ GeV and 1.0 GeV $< p_t < 2.5$ GeV and b) for inclusive Ξ^- production for 0.4 GeV $< p_t < 2.5$ GeV. The predictions of the PHOJET and PYTHIA programs are also shown.
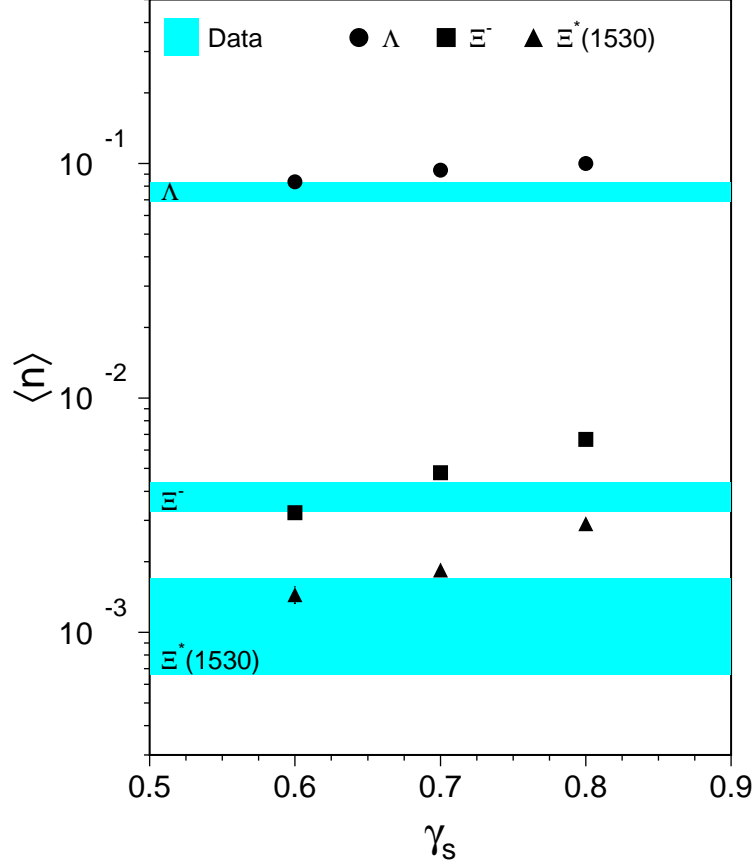
Figure 12: The extrapolated mean multiplicities $\langle n \rangle$ of Λ, Ξ^- and $\Xi^*(1530)$ baryons per two-photon event for $W_{\gamma\gamma} > 5$ GeV (horizontal bars) compared to the predictions of the thermodynamical model as a function of the strangeness suppression factor, γ_s, using as energy density the value $\rho = 0.4$ (symbols).
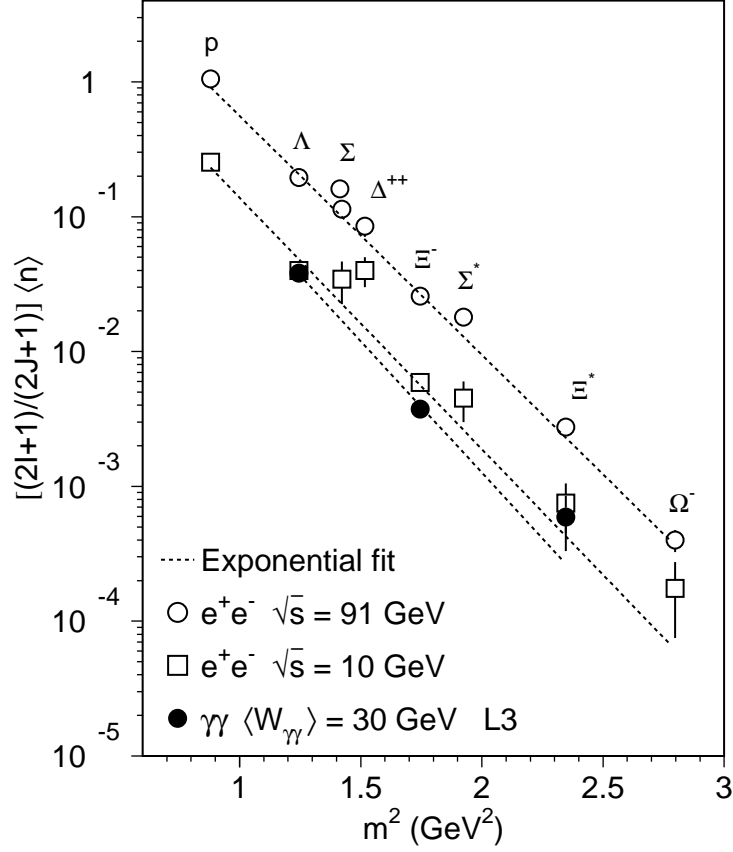
Figure 13: Weighted mean multiplicities $\left[(2J+1)/(2I+1)\right]\langle n\rangle$ as a function of the square of the baryon masses measured in two-photon reactions (solid circles) together with the data obtained in e^+e^- collisions at $\sqrt{s} = 10$ GeV (open squares) and $\sqrt{s} = 91$ GeV (open circles). The lines correspond to the fits described in the text.
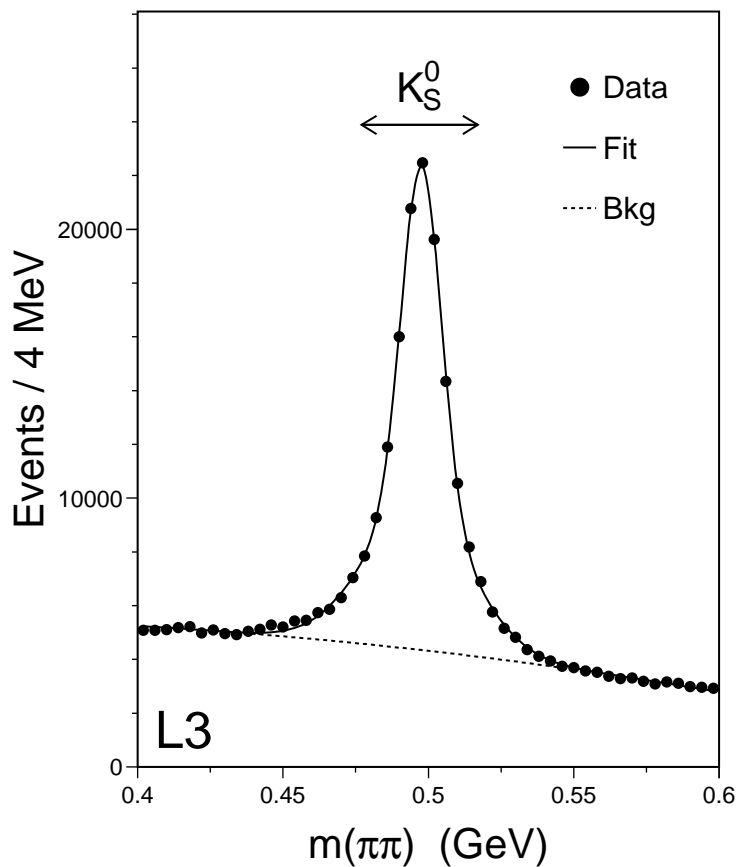
Figure 14: The effective mass of the $\pi\pi$ system. The signal is modelled with two Gaussian functions and the background by a second-order polynomial. About 140000 K_S^0 candidates are found in a ± 20 MeV window around the central value of the peak and used in the search for the θ^+ pentaquark.
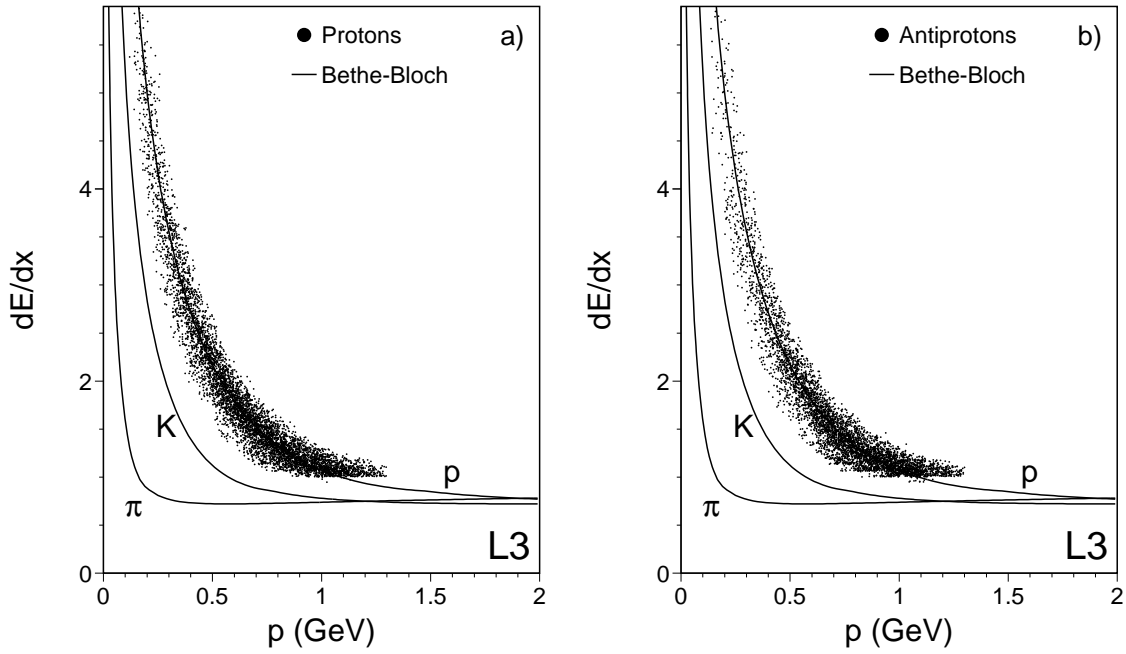
Figure 15: The dE/dx measurement as a function of the momentum for the selected a) protons and b) antiprotons, together with the calculations of the Bethe-Bloch formula for protons, kaons and pions.
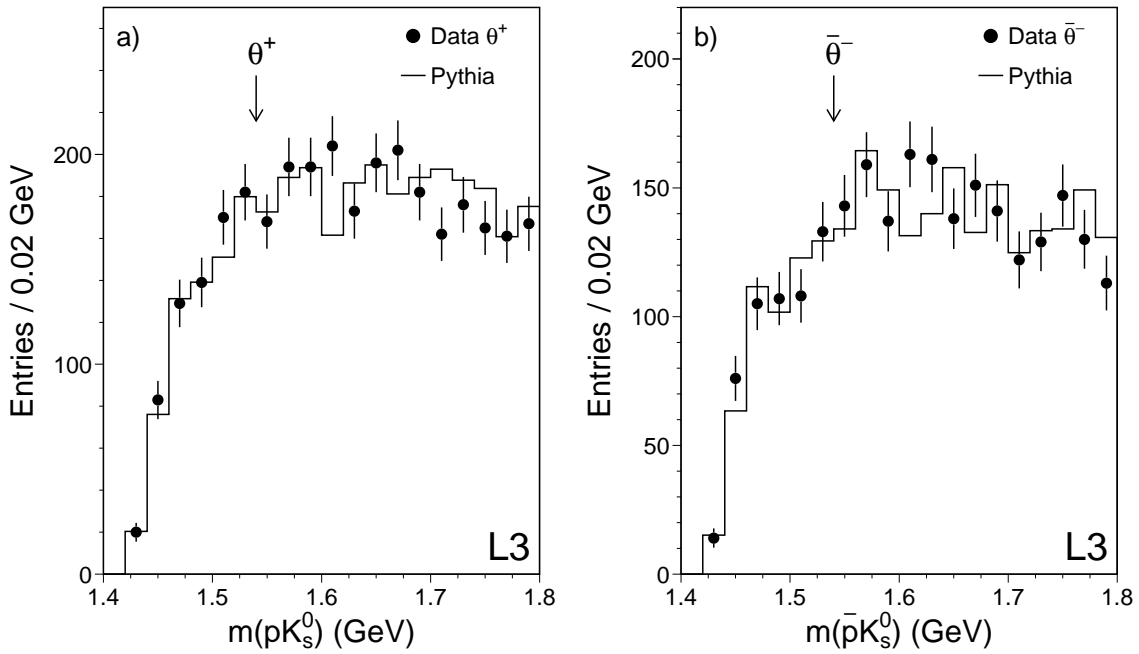

Figure 16: The mass of the pK$_S^0$ system, m(pK$_S^0$), for a) protons and b) antiprotons together with the predictions of the PYTHIA Monte Carlo. The arrow indicates the position of the expected θ^+ signal, around 1.54 GeV.
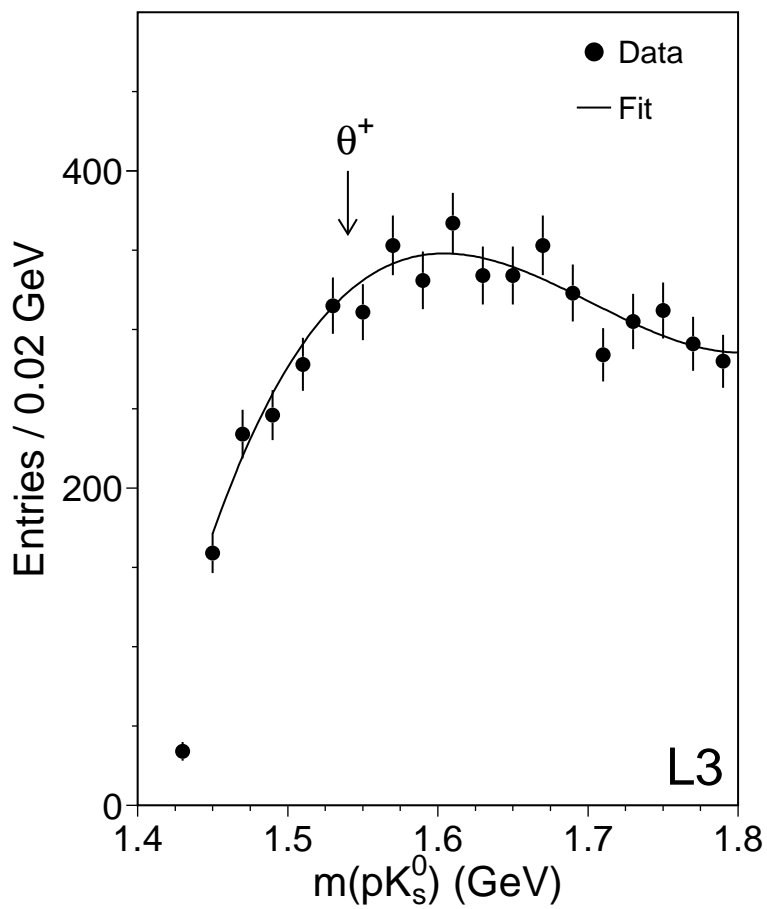
Figure 17: The mass of the pK_S^0 system, $m(pK_S^0)$, for protons and antiprotons combined together with the fit result. The arrow indicates the position of the expected θ^+ signal, around 1.54 GeV.